

Response to Anonymous Referee #1:

General comments:

This paper describes a newly developed CCD and laser-based detection system for measuring aerosol phase function.

Overall, this instrument has some advantages, such as a very simple setup and design. I believe that, if the efficacy can be shown, the idea for this instrument is a significant advance and falls under the scope of AMT.

However, I feel that there are some outstanding questions that need to be addressed before the paper can be published. These are listed below in the specific comments.

I believe that if these questions are addressed, then the paper may be publishable.

However, the following questions are crucial to the measurement and the authors may need to perform more measurements to ensure the efficacy of the instrument.

In general, the English in the paper is relatively unclear and needs to be edited.

Response: Thanks for the comments. The English has been improved in the revised manuscript.

Specific comments:

1. What is the polarization state of the laser relative to the plane of scattering?

Although the authors do not specifically address this, I suspect that they have taken this detail into consideration. The point of my comment is that the phase function of the aerosol depends on the incoming polarization of the

laser relative to the plane of scattering. The laser polarization can be oriented perpendicular to, parallel to, or somewhere in between these two positions. In order to compare the measurements to Mie theory, the polarization state must be included in the Mie calculation. This is not mentioned in the paper.

The scattered light will also be polarized and this needs to be addressed as well. For example, the detectors may detect different polarizations of light slightly differently. A flat-field calibration across the CCDs is also needed to verify that different angles of incident light to the detector are measured with equal sensitivity.

Response: This is a good question. We do consider the polarization state of the laser in this work. A quarter-wave plate was inserted above the laser to change the polarization from linear to circular. During the exposure time of the image, the circular-polarization effects mimic unpolarised light. We added the explanation of the state of polarization into the manuscript at P2L9 as:

“To change the polarization state of the laser from linear to circular, a quarter-wave plate was mounted in front of the laser emitter. During the exposure time (few minutes) of the image, the circular-polarization light can be assumed as unpolarized.”

The sensitivity of each pixel is influenced by CCD and lens. The CCD sensor we used is KAF-8300 whose quantum efficiency is about 55% at 532nm. The linear error of the CCD is about 10% according to the manual.

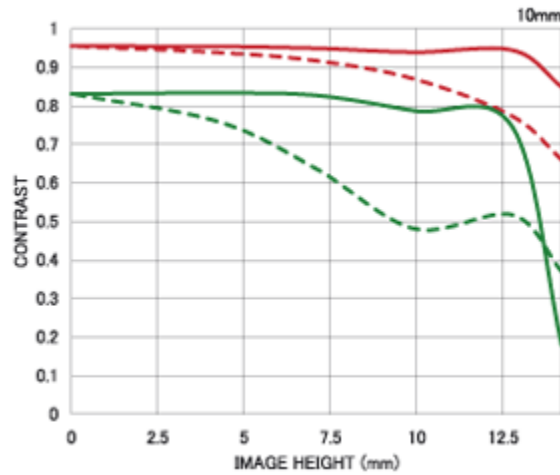


Fig.1 Modulation transfer function of Sigma 10mm F2.8 fisheye lens

The modulation transfer function of the lens we used is shown in Fig.1 (http://www.sigma-photo.co.jp/english/lens/wide/10_28/#/data). In this figure, the solid line show the performance of lens along the diagonal line. X axis shows the distance from the centre of the image. Because the diagonal line of the CCD is 22.5 mm length, the distance between the central pixels and the corner is about 11.3 mm. In this range the performance of lens is almost constant. Some parameters about the CCD and lens are added into the manuscript at P3L18 and P3L23 as:

“The quantum efficiency of the CCD is about 55% at 532nm, while the linearity error is about 10%.”

“The modulation transfer function of the lens shows that, according to the size of the CCD sensor, the difference of the sensitivities from the centre to the corner is less than 5% (http://www.sigma-photo.co.jp/english/lens/wide/10_28/#/data).”

The detailed error analysis has been added as Section 2.2.3.

2. How can the authors be sure that they are not detecting scattered light from multiple points along the laser into their CCD detectors? Although this is mentioned in the text, it is not clear that this is true.

In Figure 1, the authors show the setup, including scattering angle into the detector. But the aerosol is not constrained in any way along the path of the laser. Therefore, light scattering from a particle near the laser and from a particle at a different point along the laser beam could strike the detector at the same location.

It would be highly useful to show some raw data from the two CCD detectors for one measurement to show the relationship between the two and how the data is spliced together. At what scattering angles do the two CCD measurements overlap?

How do the authors determine the scattering angle that corresponds to each pixel position on the CCD? Is there some sort of measurement of a known scatterer that could be used to calibrate the angle, such as PSL or ammonium sulfate?

In general, it would be a good idea to perform the measurement with a known compound to better determine the efficacy of the instrument.

Response: Thanks a lot for the suggestions.

The CCD detectors are used to capture image of the laser beam. The Figure 1(b) in the revised manuscript has been added to show the image captured by CCDs. According to the principle of image formation by lenses, there is a one-to one correspondence between the image and the laser beam object ([https://en.wikipedia.org/wiki/Lens_\(optics\)\)](https://en.wikipedia.org/wiki/Lens_(optics))). The explanation has also been added at P4L2 as:

“With the mounted lens, there is a one-to-one correspondence between the image of the laser beam captured by CCDs and the laser beam object according to the principle of image formation by lenses.”

According to your suggestion, more details about the geometric measuring process and the data merging have been added in Section 2.2.1 at P4L16 and P5L16 respectively, as:

“The data acquisition of CCD-LADS is to obtain the angle-resolved scattering signals from images captured by two independent CCD systems, and then merge the signals. Firstly, the CCD-LADS is set up as the Figure 1(a) shows. The geometric relationships among the CCDs, laser emitter and light trap are measured by tape. Then the scattering angle of laser in the image should be calibrated. Firstly, the direction of the CCD cameras are adjusted to make sure that the image of laser is go through the centre of the pixel arrays of CCD. By using a beam block to block the backscattering light into the CCD, the pixel related to the 90° scattering angle can be indicated on the calibrated image (Figure 1(d)). Because of the equisolid projection is used by the lens, the distance from a point on the image on the CCD to the centre of the pixels can be represented as $R = 2f \times \sin(\theta/2)$, where θ is the angle in rad between a point in the real world and the optical axis, which goes from the center of the image through the center of the lens, f is the focal length of the lens (Miyamoto, 1964). So the scattering angle which the centre of the image related to can be calculated by substituting the distance from the pixel related to the 90° scattering angle to the centre of pixels in the calibrated image into the equation of the equisolid projection. A one-to-one correspondence between the image of laser and the scattering angle can be calibrated by this method.”

“When the angle-resolved signals from two CCDs are obtained, the change of signals with angles can be merged by following the steps below. Firstly, the minimum angle θ_1 and maximum angle θ_2 of the overlap angular region of signals from two CCDs are set as the boundary angle of data merging (shadow zone in Figure 3). θ_1 and θ_2 are always around 50° and 80°, respectively. In this region, a transform coefficient with scattering angles $T(\theta)$ is calculated,

$$T(\theta) = \frac{I_1(\theta)}{I_2(\theta)} \quad (2)$$

$I_1(\theta)$ is the signal with the scattering angle θ captured by the first CCD while $I_2(\theta)$ is that of the second CCD. The lifted signal $I_2'(\theta)$ can be calculated by multiplying $I_2(\theta)$ with the average of $T(\theta)$ (Figure 3). For the region where $\theta < \theta_1$ or $\theta > \theta_2$, the signal $I_1(\theta)$ or $I_2'(\theta)$ is used as the merged scattering signal $I(\theta)$, respectively. For the overlap region, a linear weighting average is done between $I_1(\theta)$ and $I_2'(\theta)$,

$$I(\theta) = \frac{\theta_2 - \theta}{\theta_2 - \theta_1} \times I_1(\theta) + \frac{\theta - \theta_1}{\theta_2 - \theta_1} \times I_2'(\theta).$$

Using the method above, the merged signals with scattering angles $I(\theta)$ can be estimated.”

The CCD-LADS is designed as an open path system to measure the ambient aerosols directly. Using a known compound just like PSL to calibrate the system is difficult because there is not a cavity in this system.

3. More detail is needed regarding many aspects of the study. There needs to be more information regarding how the Mie calculations were performed. What was the refractive index used? Were the size distributions from the SMPS?

Response: Thanks for your suggestion. We have added more information about the Mie calculation we used at P8L19, as:

“Combining the particle number size distributions measured with SMPS/APS and the mass concentration of black carbon aerosols measured with AE51 which are shown in Figure 6 into a modified Mie-scattering model, the aerosol optical properties including the aerosol phase function could be modelled (Ma et al., 2011). In this study (both laboratory and field study), the refractive index used for black carbon component is $1.95-0.79i$ (Seinfeld and Pandis, 2006), and for non-absorbing component is $1.53-10^{-7}i$ (Wex et al., 2002). The mass ratio between two different mixing states (external or core-shell, which means the different mixing way of black carbon and non-absorbing aerosols) of black carbon aerosols is assumed to be 1:1 according to the result of Ma et al. (2012).”

4. The instrument will measure scattered sunlight when used during daylight hours. Using a 532 nm filter in front of the cameras will block much of the scattered sunlight, but the sunlight near 532 nm will be scattered by the particles and will reach the detector. Was there any attempt to block the sun from reaching the particles? For example, could a dark curtain or sampling box be used?

Response: Thanks for the suggestions. Because the scattering phase function of the ambient aerosols is supposed to be observed, the noise from the

sunlight is an obvious issue indeed. Because the signal to noise ratio is lower during the daytime, actually we just used the nocturnal data to analyse. This issue was mentioned at the last sentence of Section 2.1. According to your comment, a further sentence has been added at P4L12 as:

“Currently, the CCD-LADS system can just estimate the nocturnal aerosol scattering phase function.”

5. Fluctuating temperature in the ambient measurement will likely cause fluctuations in the laser alignment during the measurements. Also, temperature fluctuations could affect the CCD efficiencies. Were the CCD cameras electronically cooled or was the temperature stabilized in any way?

Response: After the system deployed, the laser alignment would be checked in every image. It seemed that the fluctuating temperature do not influence the laser alignment during night time in our observations. The CCD camera has an air-cooling unit. We added the description about this unit and the related setting at P3L18 and P4L28 as:

“This camera has an air-cooling unit to control the temperature of CCD.”

“At the beginning of the measurement, the CCDs are cooled down to -15°C to minimize the noise from dark current.”

6. The authors claim that a significant portion of the particles measured were biomass burning particles. These particles could absorb a significant fraction of light. Was the absorption considered in the Mie calculations or was only scattering considered?

Response: Both scattering and absorption are considered in the Mie calculation. An aethalometer was used in the observations to measure the absorption coefficient. The detailed description about the parameter used in

the Mie calculation have been added in the manuscript. Please see the response to specific comment 3.

7. Ambient gases, such as nitrogen dioxide and ozone could absorb a significant fraction of light. It would be useful on Page 4, Line 20, for example, to discuss more detail in the assumption that the transmittance of the laser is 1.

Response: The maximum mixing ratio of NO₂ and O₃ are about 100ppb and 200ppb in the North China Plain, respectively (Xu et al., 2011). The absorption cross sections of these two gases on the 532nm wavelength are measured in the past studies (Dixon, 1940; Burrows et al., 1999). According to the parameters in these studies, the maximum absorption coefficient of NO₂ is about 20Mm⁻¹, which have the same order with the scattering coefficient of air molecules. The maximum absorption coefficient of O₃ is about 2Mm⁻¹ which can be ignored compared with the absorption of NO₂ on this wavelength. According to the area that the CCD-LADS covers, the extinction coefficient of air molecules which including the scattering coefficient and the absorption coefficient of all the ambient gases can lead to a transmittance of 99.94% at most. In some extreme pollution processes, the extinction coefficient of aerosols may be exceeded 2000 Mm⁻¹ which can lead to a transmittance of 96.85% (Ma et al., 2011). Considering this issue, a threshold of visibility has been added to evaluate if the assumption used or not. The sentences have been added at P6L4 as:

“Depend on the area that the CCD-LADS covers, the longest distance between CCD cameras and the laser beam is less than 8m. In this range, an assumption that $\tau_Z = \tau_R = 1$ can be established with a threshold that the visibility should be larger than 1.5km. The correlation between the visibility and extinction coefficient k_{ex} can be expressed as $k_{ex} = 3/visibility(km)$ (Chen et al., 2012) which means that the

assumption can be established if k_{ex} is smaller than 2km^{-1} . In some extreme pollution processes while both aerosols and polluted gases are in large quantities (Ma et al., 2011; Xu et al., 2011), the scattering and absorption of aerosols and gases (NO_2 (Dixon, 1940), O_3 (Burrows et al., 1999), etc.) may lead to a marvelous k_{ex} . If the k_{ex} is more than 2km^{-1} , the assumption cannot be applied while the transmittance can be calculated with the measurement of visibility.”

8. The entire discussion of the retrieval algorithm is not clear (Section 2.2.2). More detail is needed. Please describe exactly how the retrieval algorithm works. Why is the retrieval needed? You are measuring the phase function, correct? Why would you need to retrieve it?

Response: Thanks for the suggestion. The direct measured parameter of the CCD-LADS is the scattering phase function of the ambient air mass including air molecules and aerosols. The retrieval algorithm is to obtain the scattering phase function of ambient aerosols. The difference between the aerosol phase function obtained with the retrieval algorithm and measured directly is shown in Figure 7. We rewrite the Section 2.2.2 as:

“Figure 2 shows the flow chart of the retrieval algorithm to determine $p(\theta)$ from CCD-LADS measurements. According to the geometric structure of the CCD-LADS, the echo equation of CCD-LADS can be figured firstly,

$$I(\theta) = N_0 \tau_Z \tau_R \beta(\theta) \quad (4)$$

where $\beta(\theta)$ is the scattering function of atmospheric air molecules and aerosols, τ_Z and τ_R are the transmittances on the optical paths of laser emitting and scattering respectively, N_0 is the calibration factor that depends on the optical efficiency of the instrument. Depend on the area that the CCD-LADS covers, the longest distance between CCD cameras and the laser beam is less than 8m. In this range, an assumption that $\tau_Z = \tau_R = 1$ can be established with a threshold that the visibility should be larger than 1.5km. The correlation between the visibility and extinction coefficient k_{ex} can be expressed as $k_{ex} = 3/\text{visibility}(\text{km})$ (Chen et al., 2012) which means that the assumption can be established if k_{ex} is

smaller than 2km^{-1} . In some extreme pollution processes while both aerosols and polluted gases are in large quantities (Ma et al., 2011; Xu et al., 2011), the scattering and absorption of aerosols and gases (NO_2 (Dixon, 1940), O_3 (Burrows et al., 1999), etc.) may lead to a marvelous k_{ex} . If the k_{ex} is more than 2km^{-1} , the assumption cannot be applied while the transmittance can be calculated with the measurement of visibility. With the assumption, equation (4) can be transformed to $I(\theta) = N_0\beta(\theta)$.

Scattering phase function $p(\theta)$ is the normalized angular distribution of the scattering function,

$$p(\theta) = \frac{4\pi\beta(\theta)}{\int_0^{180} \beta(\theta)d\theta} = \frac{4\pi I(\theta)}{\int_0^{180} I(\theta)d\theta} \quad (5)$$

So the scattering phase function can be calculated directly from $I(\theta)$ measured by CCD-LADS.

If the scattering function of aerosols $\beta_{aero}(\theta)$ is known, the $p(\theta)$ can be calculated. Therefore, a retrieval algorithm is built to separate the scattering signals with angles into the scattering of aerosols and air molecules (shown in the dashed box in Figure 4).

As the first step, the scattering coefficient of air molecules at near surface level k_{sc-air} is calculated with the density of atmosphere by a Rayleigh scattering model,

$$k_{sc-air} = \frac{8\pi^3(m^2-1)^2}{3n_{air}\lambda^4} \quad (6)$$

where n_{air} is the number density of air molecules which depends on the surface pressure and temperature measured by the weather station, m is the index of refraction of atmosphere, which depends on n_{air} and the wavelength of the laser λ . The hemispheric backscattering coefficient of air molecules $k_{bsc-air}$ is a half of k_{sc-air} (Bohren and Huffman, 2008).

To resolve the ratio between the air molecules and the total hemispheric scattering $R_{air} = \frac{k_{bsc-air}}{k_{bsc-air} + k_{bsc-aero}}$, the hemispheric backscattering coefficient of aerosols $k_{bsc-aero}$ are measured with an integrating nephelometer here.

To solve the intensity of the total hemispheric backscattering scattering signals I_{bsc} , the angle-resolved scattering signals should be integrated from 90° to 180° scattering angle. Because of the detective angular range of CCD-LADS is $10^\circ - 170^\circ$, the angular truncation correction is necessary to resolve the hemispheric scattering intensity. For the backward angular truncation, the scattering intensity in that range

is assumed to be equal to the scattering intensity at the largest scattering angle that CCD-LADS can measured. After the correction above, the corrected intensity $I'(\theta)$ is used to obtain I_{bsc} ,

$$I_{bsc} = \int_0^{2\pi} \int_{\pi/2}^{\pi} I'(\theta) \sin \theta d\theta d\varphi \quad (7)$$

Then the angle-resolved scattering signals of air molecules can be calculated with a molecular phase function (Bohren and Huffman, 2008),

$$I_{air}(\theta) = \frac{3(1+\cos^2 \theta)}{4} \times \frac{I_{bsc} \times R_{air}}{2\pi} \quad (8)$$

where $I_{air}(\theta)$ is the calculated angle-resolved scattering signals of air molecules. According to equation (4), the aerosol phase function $p_{aero}(\theta)$ can be estimated,

$$p_{aero}(\theta) = \frac{4\pi(I(\theta) - I_{air}(\theta))}{\int_0^{180} (I(\theta) - I_{air}(\theta)) d\theta} \quad (9)''$$

9. Error bars (uncertainties) of the measured phase functions are needed to better understand the overlap between the models and measurements (in Figure 4, for example).

Response: We show the standard deviation of CCD-LADS results in the field measurements in the last version of manuscript. Following this comment, the error bars of the laboratory results have also been added. Please see Figure 7 in the revised manuscript and Section 3.1. Section 2.2.3 has been added to analyse the uncertainties in the measurement.

Technical corrections:

In general, there are not enough citations to the literature in the introduction. For example, Bohren and Huffman should be cited for Mie theory. The IPCC report should be cited for the first sentence (Page 1, Line 20). There are more field measurements that used an integrating nephelometer. Overall, more citations are needed.

Response: Thanks for the comment. More citations have been added including Bohren and Huffman (2008), IPCC assessment report 5 (Pachauri et al., 2014) and the nephelometer works (Heintzenberg et al., (1996) etc.) at P2L1, P1L21 and P1L22.

Throughout the paper, “figure” should be capitalized as “Figure 1”.

Response: Thanks. It has been corrected.

N_0 and T are both used as symbols for transform coefficient (Page 4, Lines 6 and 19). How are these different?

Response: Thanks for your suggestion. These two parameters are independent. The name of N_0 have been changed to “calibration factor” to distinguish with T .

Page 1, Line 24 should read “The aerosol phase function. . .”.

Response: Thanks. It has been corrected.

Page 2, Line 5 should read “A plane mirror was placed at that point and reflected the scattering signals. . .”

Response: Thanks. It has been corrected.

Page 2, Line 7: Is “linearity” correct? If so, please explain.

Response: Thanks for the comment. That word which is a typo has been deleted.

Page 2, Line 28. “mainly” is not needed. More information is needed about the laser. The make, model, etc. is needed.

Response: Thanks. “mainly” was used because the quarter-wave plate was also considered as a part of the emitting system. More information about the laser has been added at P3L9 as:

“The transverse mode is near TEM₀₀. The M₂ factor is less than 2.0 while the divergence of beam is less than 2.0mrad. The diameter at the aperture is 3.0mm.”

Page 3, Line 20 should read “The CCD-LADS system covers an area 12 m long and 1 m wide.”

Response: Thanks. It has been corrected.

Page 3, Line 21. How is the background noise measured? It would be useful to show a plot of the signals measured during the daytime and nighttime. Also, why is the noise so much higher in the daytime? See the comment above regarding the filters above. I suspect that you have a large portion of ambient light being scattered by the particles. Depending on the angle of the sun, this could affect the ambient measurements.

Response: Thanks for the suggestion again. Currently, the CCD-LADS system can just estimate the nocturnal aerosol scattering phase function. Please see the response to specific comment 4. During the night time, the background noise can be subtracted by the normal fitting of signals. This process has been added in Section 2.2.1 at P5L6 as:

“After image captured, the scattering light of the laser beam are separated from the background noise in the image as the follow steps. Firstly, the central axis of the scattering signals of laser beam is fitted in the

program (the red line shown in Figure 2(b)). Then the intensities of image on the perpendicular of this central axis (the blue line shown in Figure 2(b)) are fitted with a normal distribution,

$$f(x) = I_0 + I \times \frac{1}{\sqrt{2\pi}\sigma} \exp\left(-\frac{(x-\mu)^2}{2\sigma^2}\right) \quad (1)$$

where I_0 is the intensity of the background noise, I is the intensity of the scattering signal of the laser beam related to one scattering angle, x represents the distance between the pixel on the perpendicular and on the central axis of the scattering signals, σ and μ are the fitting parameters of the normal distribution. Combining with the calibrated one-to-one correspondence between the image of laser and the scattering angle, the angle-resolved scattering signals is obtained with the above steps of data acquisition.”

Page 4, Lines 8-13. More detail is needed about the linear weighting and the data processing in general.

Response: Thanks. More details have been added and Section 2.2.1 have been rewritten. Please see the new version of the manuscript.

Page 4, Line 30. The authors state that the hemispheric backscattering is half of the full scattering. This is true for Rayleigh scattering, but it depends on the polarization of the light. Bohren and Huffman, or a Rayleigh scattering calculation needs to be cited here.

Response: The laser is seemed as unpolarised by using a quarter-wave plate. Please see the response to specific comment 1. The citation has been added at P6L22.

Page 5, Lines 1-9. This section is very confusing. Was a separate measurement of the air molecule scattering measured by an integrating nephelometer during this study? More detail is needed. What is meant by “the percentage of air scattering”, for example? See the comment above.

Response: Thanks for the suggestion. The air molecule scattering is calculated by the formula of Rayleigh scattering with the measured temperature and relative humidity. “the percentage of air scattering” means the fraction of air scattering coefficient in the total scattering coefficient ($\frac{k_{sc-air}}{k_{sc-air}+k_{sc-aero}}$). “the percentage of air scattering” has been expanded as “the percentage of air scattering in total scattering” in the revised manuscript. The Section 2.2.2 has been rewritten according to your suggestion. Please see the response to the specific comment 8.

Page 6, Line 13. What is the external/core-shell ratio of 1:1? What does this mean? 1:1 core and shell ratio by volume?

Response: External state and core-shell state are different mixing states of black carbon (BC). The mixing state will influence the optical properties of aerosols. In the Mie calculation, the BC mass ratio of different mixing state is needed. The detailed descriptions of Mie calculation are added. Please see the response to specific comment 3.

Page 6, Line 23. The explanation that the scattering abilities of aerosol particles and gas molecules match better in the back scatter than the forward scatter is not clear. In the phase function, the Rayleigh and Mie scattering generally match in the forward and reverse directions (0 and 180 degrees).

Response: Thanks for your comment. Here the “scattering abilities” should be instead by “scattering coefficients”. In general, the scattering coefficient of aerosol is much higher than the scattering coefficient of air molecule. Based on this background, the back-scattering coefficients of aerosol and air molecule are closer to each other than the forward-scattering coefficients

according to the different patterns of the phase function of Rayleigh and Mie scattering. The sentence has been rewritten at P9L5 as:

“The reason of this phenomenon is that the scattering coefficients of aerosols and air molecules are closer to each other for the backward scatter than for the forward scatter based on the background that the total scattering coefficient of aerosols is always much higher than of air molecules.”

Page 6, Line 25 and Figure 4. Biomass burning aerosol is not shown on the graph. Also, this needs a reference for the discussion about biomass burning size, absorption, etc.

Response: The scattering phase function of the “biomass burning” aerosol from the Cloud-Aerosol Lidar and Infrared Pathfinder Satellite Observations (CALIPSO) aerosol products (Omar et al., 2009) has been added in Figure 7 in the revised manuscript. The description of the aerosol classification from CALIPSO and the typical characteristics of biomass burning aerosols have been added with the related reference at P8L27 and P9L9, as:

“The CALIPSO aerosol classifications are based on the cluster analysis of the Aerosol Robotic Network (AERONET) measurements to determine characteristic aerosol types (Omar et al., 2005).”

“Compared with the other aerosol types, the “biomass burning” aerosol represents a better absorption ability due to the larger percentage of black carbon aerosol and organic aerosol, and also a smaller effective diameter around 100nm (Omar et al., 2005; Rissler et al., 2006; Zhu et al., 2017).”

Page 7, Line 2. The authors state that the difference “Is not obvious”, but there is clearly a difference between the Mie model and the measurement in Figure 5. This is not clear.

Response: We deleted the “Is not obvious” in the revised manuscript, rewritten it as “the average difference in the absolute values between these two $p(\theta)$ is less than 10%” at P9L18.

Page 7, Line 13. Why was the instrument limited to 30-160 degrees because of the ambient conditions?

Response: The mobile laboratory was deployed on the roof of a building. To compare with the other in-situ measurements, the CCD-LADS was also installed on the roof. But there were limited space for a standard CCD-LADS system. So we shorten the distance between the laser and the beam trap, which cause the limitation of the detection range.

Page 7, Line 16. It is more correct to say that the particles will exhibit hygroscopic growth rather than “grow up”. Also in Line 18, why was the data collected at RH >70% eliminated? How was 70% RH chosen? Many particles exhibit water uptake at lower relative humidities. Biomass burning aerosol is highly hygroscopic and shows continuous growth. 70% seems to be arbitrarily chosen.

Response: Thanks. “Grow up” has been instead by “exhibit hygroscopic growth” at P10L1. We chose the 70% RH because the deliquescence relative humidity is always beyond 73% in this region in our previous study (Kuang et al., 2016). The ratio of aerosol light scattering coefficients at 70% RH and at dry condition is about 1.3 (Chen et al., 2014), which will not influence the result too much. If a 50% or 60% RH is chosen, the comparison between CCD-LADS measurements and Mie calculations may be better, but the data quantity will also decrease.

Page 7, Line 18. It is better to say “eliminated” than “kicked off”.

Response: Thanks. It has been corrected.

Page 7, Line 26. What is meant by better stability? Was the data less noisy?
This is not clear.

Response: Compared to the Aurora 4000 measurements, the deviation of the CCD-LADS measurements is significantly less obvious (Fig.2). That’s the reason why we use “better stability” as an advantage of CCD-LADS.

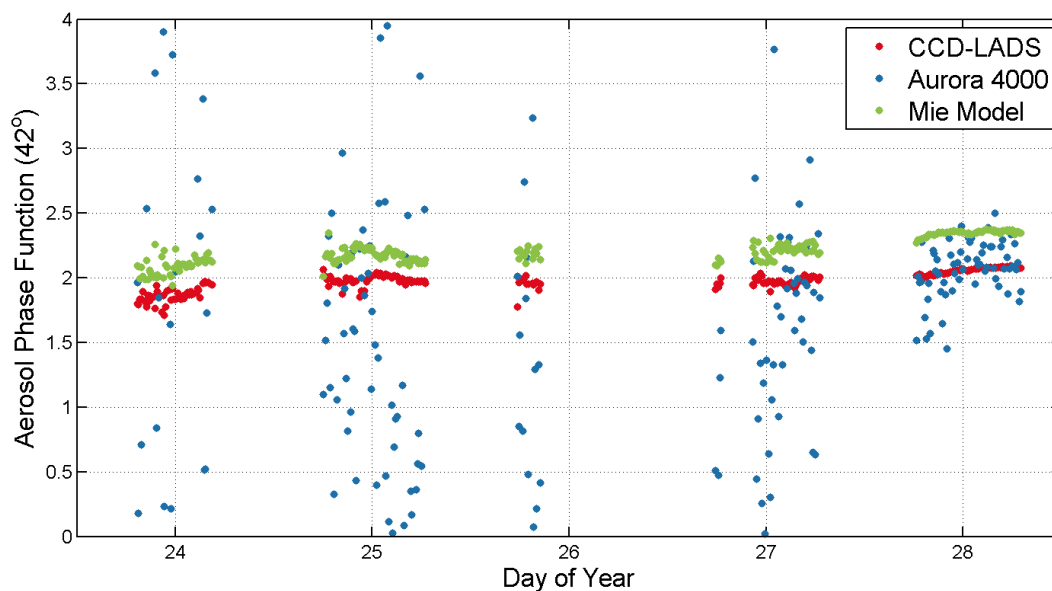


Fig. 2 Comparison between aerosol phase function at 42° scattering angle obtained from CCD-LADS measurements, Aurora 4000 measurements and modelled with modified Mie model.

Page 8, Line 18. What is meant by “steadier”?

Response: “steadier” is as the same meaning as “better stability” that we explained in the last response.

Figure 3: The data shown here was not collected by the CCD-LADS instrument that is the focus of this paper. Why is this data shown? Was it used in the Mie calculation to compare to the CCD-LADS measurements?

Response: Yes. These characteristics are used in the Mie calculation and also the retrieval algorithm to determine the aerosol phase function with CCD-LADS measurements. The explanation of this figure has been added at P8L19 as:

“Combining the particle number size distributions measured with SMPS/APS and the mass concentration of black carbon aerosols measured with AE51 which are shown in Figure 6 into a modified Mie-scattering model, the aerosol optical properties including the aerosol phase function could be modelled (Ma et al., 2011).”

References:

Bohren, C. F., and Huffman, D. R.: Absorption and scattering of light by small particles, John Wiley & Sons, 2008.

Burrows, J. P., Richter, A., Dehn, A., Deters, B., Himmelmann, S., Voigt, S., and Orphal, J.: ATMOSPHERIC REMOTE-SENSING REFERENCE DATA FROM GOME—2. TEMPERATURE-DEPENDENT ABSORPTION CROSS SECTIONS OF O₃ IN THE 231–794NM RANGE, *Journal of Quantitative Spectroscopy and Radiative Transfer*, 61, 509-517, [http://dx.doi.org/10.1016/S0022-4073\(98\)00037-5](http://dx.doi.org/10.1016/S0022-4073(98)00037-5), 1999.

Chen, J., Zhao, C. S., Ma, N., and Yan, P.: Aerosol hygroscopicity parameter derived from the light scattering enhancement factor measurements in the North China Plain, *Atmos. Chem. Phys.*, 14, 8105-8118, [10.5194/acp-14-8105-2014](https://doi.org/10.5194/acp-14-8105-2014), 2014.

Dixon, J. K.: The Absorption Coefficient of Nitrogen Dioxide in the Visible Spectrum, *The Journal of Chemical Physics*, 8, 157-160, [10.1063/1.1750622](https://doi.org/10.1063/1.1750622), 1940.

Heintzenberg, J., and Charlson, R. J.: Design and Applications of the Integrating Nephelometer: A Review, *Journal of Atmospheric and Oceanic Technology*, 13, 987-1000, 10.1175/1520-0426(1996)013<0987:DAAOTI>2.0.CO;2, 1996.

Kuang, Y., Zhao, C. S., Ma, N., Liu, H. J., Bian, Y. X., Tao, J. C., and Hu, M.: Deliquescent phenomena of ambient aerosols on the North China Plain, *Geophysical Research Letters*, n/a-n/a, 10.1002/2016gl070273, 2016.

Ma, N., Zhao, C. S., Nowak, A., Müller, T., Pfeifer, S., Cheng, Y. F., Deng, Z. Z., Liu, P. F., Xu, W. Y., Ran, L., Yan, P., Göbel, T., Hallbauer, E., Mildenerger, K., Henning, S., Yu, J., Chen, L. L., Zhou, X. J., Stratmann, F., and Wiedensohler, A.: Aerosol optical properties in the North China Plain during HaChi campaign: an in-situ optical closure study, *Atmos. Chem. Phys.*, 11, 5959-5973, 2011.

Omar, A. H., Winker, D. M., Vaughan, M. A., Hu, Y., Trepte, C. R., Ferrare, R. A., Lee, K.-P., Hostetler, C. A., Kittaka, C., Rogers, R. R., Kuehn, R. E., and Liu, Z.: The CALIPSO Automated Aerosol Classification and Lidar Ratio Selection Algorithm, *Journal of Atmospheric and Oceanic Technology*, 26, 1994-2014, 10.1175/2009jtecha1231.1, 2009.

Pachauri, R. K., Allen, M. R., Barros, V. R., Broome, J., Cramer, W., Christ, R., Church, J. A., Clarke, L., Dahe, Q., Dasgupta, P., Dubash, N. K., Edenhofer, O., Elgizouli, I., Field, C. B., Forster, P., Friedlingstein, P., Fuglestvedt, J., Gomez-Echeverri, L., Hallegatte, S., Hegerl, G., Howden, M., Jiang, K., Jimenez Cisneroz, B., Kattsov, V., Lee, H., Mach, K. J., Marotzke, J., Mastrandrea, M. D., Meyer, L., Minx, J., Mulugetta, Y., O'Brien, K., Oppenheimer, M., Pereira, J. J., Pichs-Madruga, R., Plattner, G.-K., Pörtner, H.-O., Power, S. B., Preston, B., Ravindranath, N. H., Reisinger, A., Riahi, K., Rusticucci, M., Scholes, R., Seyboth, K., Sokona, Y., Stavins, R., Stocker, T. F., Tschakert, P., van Vuuren, D., and van Ypserle, J.-P.: *Climate Change 2014: Synthesis Report. Contribution of Working Groups I, II and III to the Fifth Assessment Report of the Intergovernmental Panel on Climate Change*, edited by: Pachauri, R. K., and Meyer, L., IPCC, Geneva, Switzerland, 151 pp., 2014.

Xu, W. Y., Zhao, C. S., Ran, L., Deng, Z. Z., Liu, P. F., Ma, N., Lin, W. L., Xu, X. B., Yan, P., He, X., Yu, J., Liang, W. D., and Chen, L. L.: Characteristics of pollutants and their correlation to meteorological

conditions at a suburban site in the North China Plain, *Atmos. Chem. Phys.*, 11, 4353–4369, 10.5194/acp-11-4353-2011, 2011.

Development and validation of a CCD-laser aerosol detective system for measuring the ambient aerosol phase function

Yuxuan Bian^{1,2}, Chunsheng Zhao², Wanyun Xu³, Gang Zhao², Jiangchuan Tao², Ye Kuang²

¹State Key Laboratory of Severe Weather, Chinese Academy of Meteorological Sciences, Beijing, 100081, China

²Department of Atmospheric and Oceanic Sciences, School of Physics, Peking University, Beijing, 100871, China

³State Key Laboratory of Severe Weather & Key Laboratory of Atmospheric Chemistry of CMA, Chinese Academy of Meteorological Sciences, Beijing, 100081, China

Correspondence to: Chunsheng Zhao (zcs@pku.edu.cn)

Abstract. Aerosol phase function represents the angular scattering property of aerosols, which is crucial for understanding the climate effects of aerosols that have been identified as one of the largest uncertainties in the evaluation of radiative forcing. So far, there is a lack of instruments to measure the aerosol phase function directly and accurately in laboratory studies and in-situ measurements. A portable instrument with high angular range and resolution has been developed for the measurement of the phase function of ambient aerosols in this study. The charge-coupled device-laser aerosol detective system (CCD-LADS), which measures the aerosol phase function both across a relatively wide angular range of 10° - 170° and at a high resolution of 0.1° . The system includes a continuous laser, two charge-coupled device cameras and the corresponding fisheye lenses. The CCD-LADS was validated by both a laboratory study and a field measurement. The comparison between the aerosol phase function retrieved from CCD-LADS and Mie-scattering model shows good agreement. Compared with the TSI polar nephelometer, CCD-LADS has the advantages of wider detection range and better stability.

1 Introduction

The climate effect of aerosol optical properties is one of the greatest uncertainties in our understanding about the climate change (Pachauri et al., 2014). Instruments such as the integrating nephelometer were often used to measure the aerosol scattering coefficient in laboratory studies and field campaigns (Anderson et al., 1996; Heintzenberg and Charlson, 1996; Ma et al., 2011; Müller et al., 2011; Ma et al., 2011; Tao et al., 2014). However, besides the total scattering coefficient, the distribution of aerosol scattering at different directions also has significant impact on the direct climate effect of aerosols (Kuang et al., 2015; Kuang et al., 2016b). The Aerosol-aerosol phase function ($p(\theta)$) is defined to describe the angular distribution of the aerosol scattering intensity (Hulst, 1957). $p(\theta)$ is one of the important properties determining the contribution of aerosols to the radiative balance of the atmosphere (Andrews et al., 2006). Some parameters such as the asymmetry parameter and the hemispheric backscatter fraction estimated from $p(\theta)$ are of great importance to the retrieval of remote sensing measurements and in the simulation of atmospheric radiative transfer models (Muñoz et al., 2002). If the particle is assumed to be spherical, there is a comprehensive theory named the Mie scattering theory to describe the

characteristics of aerosol scattering, when the particle size is in the same scale with the wavelength of scattering light (Bohren and Huffman, 2008). $p(\theta)$ can also be calculated with the size and complex refractive index of particles by the Mie theory (Kim et al., 2010).-

In past years, different research groups have developed several versions of polar nephelometers to measure how the scattering

intensities of aerosol particles, cloud droplets and ice crystals changes with scattering angle. Muñoz et al. (2001, 2010, 2011) mounted a photomultiplier tube (PMT) on a mechanical arm which can rotate around a point on the laser light path in the same plane with the laser beam to change the scattering angle of the signal captured by the PMT. Castagner and Bigio (2006, 2007) focused the light scattered at a single spot with different scattering angles to another single spot by using two parabolic reflectors next to the light path. A plane mirror was placed at that point to reflect the scattering signals with different angles to a PMT by rotation. These two styles of instruments measured the angular distribution of scattering signals by using the rotational mechanism. This design will lead to an obvious uncertainty because the signals were not measured simultaneously.

Barkey et al. (2002, 2007) made the sample flow perpendicular and intersect with the light path. Then many PMTs were mounted around the point of intersection in the same plane with the laser beam to capture the scattering signal from different scattering angles. Castagner and Bigio (2006, 2007) focused the light scattered at a single spot with different scattering angles to another single spot by using two parabolic reflectors next to the light path. A plane mirror was settled placed at that point and reflect the scattering signals with different angles to a PMT by rotation. The signals with different scattering angles were measured at the same time with this design, however, the angular resolution which is limited to larger than 8° per point is relatively low because the PMTs cannot be mounted too close to each other. Curtis et al. (2007, 2008) used an ellipsoidal mirror to reflect the scattering light to a linearity charge-coupled device (CCD) detector for the detection of aerosol phase function. By using CCD as detector, This method can offer a better angle and time resolution at a wider range of scattering angles than the other methods above. It just needs one detector and there is no need to move the detector during the measurement. However, the structure of this design is too complicated to be used in field measurements.

Recently, McCrowey et al. (2013) developed a miniaturized polar nephelometer, which can be used in the in-situ measurement based on the techniques of Curtis et al. (2007) and can then be calibrated in the laboratory using polystyrene latex (PSL) standard particles. A comparison between the results measured from this instrument and calculated from a Mie model showed a good agreement. The detection range of this instrument is from 20 to 155° scattering angle. Besides these studies, the Aurora 4000 polar nephelometer (Ecotech Pty Ltd., Australia) is currently the only commercial instrument that can measure the aerosol phase function. This product has a structure similar to that of the integrating nephelometer, while a backscatter shutter that is able to be positioned at any angle between 10 - 90° is mounted in the cavity to help the nephelometer measuring the light scattering from that angle, through to 170° . The Aurora 4000 can just measure the aerosol phase function in a scattering angle range of 0 - 90° for dry aerosols. These two instruments can be used to measure the scattering phase function of dry aerosols in in-situ measurements.

In this paper, A novel instrument named charge-coupled device-laser aerosol detective system (CCD-LADS) based on the CCD imaging principle and the optical structure of the fisheye lens is developed to measure the ambient aerosol phase function in the field measurement at a wider range of detection angles and a higher accuracy. The validation in both laboratory and field measurement shows the ability of the CCD-LADS to measure the aerosol phase function.

2 Instrumentation and Methodology

2.1 Design of instrument

The CCD-LADS includes several main components: a high power continuous laser emitter, two CCD cameras, optical filters and fisheye lenses. The laser and CCD cameras are mounted on tripods and controlled by a laptop. Each component is portable and on a scale of a few cubic ~~decimeters~~decimetres.

10 The emitting system of the CCD-LADS is mainly built with a solid continuous laser emitter. Nd: YAG is used as the solid laser material as the wavelength of the emitter is 532-nm. The transverse mode is near TEM₀₀. The M₂ factor is less than 2.0 while the divergence of beam is less than 2.0 mrad. The diameter at the aperture is 3.0 mm. The power of the laser is 1-W. To change the polarization state of the laser from linear to circular, a quarter-wave plate was mounted in front of the laser emitter. During the exposure time (few minutes) of the image, the circular-polarization light can be assumed as unpolarised.

15 The receiving system of CCD-LADS has three main parts, the CCD cameras, the optical filters and the fisheye lenses. The SBIG model STF-8300 CCD imaging camera, which has the KAF-8300 CCD sensor (ON Semiconductor, Phoenix, AZ, USA) is used. The area array (17.96*13.52 mm) of pixels has 8.3 million (3326*2504) effective pixels, while each pixel is a square 5.4 μm on a side. The exposure time is from 0.1 s to 1 h. The A/D converter is 16 bit. Due to its outstanding performance, this product is often used in astronomical measurements and also measurements in the other research areas (Coenen et al., 2015).

20 The quantum efficiency of the CCD is about 55% at 532 nm, while the linearity error is about 10%. This camera has an air-cooling unit to control the temperature of CCD.

The fisheye lens (Sigma Corp., Japan) has a 10 mm focus length and a F2.8 aperture. When this lens is used with a Nikon camera, the field of view can be 180°. Because of the size of the CCD arrays, when this lens is used with the STF-8300 camera, the field of view is about 120°. The equisolid projection, which means that the solid angle of the object is directly proportional

25 to the area on the CCD arrays, is used by this lens (Miyamoto, 1964). The modulation transfer function of the lens shows that, according to the size of the CCD sensor, the difference of the sensitivities from the centre to the corner is less than 5% (http://www.sigma-photo.co.jp/english/lens/wide/10_28/#/data).

To filter out the background noise from the sky radiation, an optical filter (Thorlabs, Newton, NJ, USA) is mounted between the CCD camera and the lens. The filter has a 532 \pm 2-2 nm wavelength, and a 10 \pm 2-2 nm full width at half maximum, while
30 the minimum transmission at the peak is 70%.

Figure 1(a) is the sketch map of the geometric relationship of CCD-LADS. The laser is emitted horizontally, while a beamlight trap is used to receive the laser beam on the other side. Besides the laser beam, two CCD cameras with fisheye lenses are installed at the same altitude with the laser to capture the scattering signal from the laser beam, while the directions of the cameras are forward and backward, respectively. With the mounted lens, there is a one-to-one correspondence between the image of the laser beam captured by CCDs and the laser beam object according to the principle of image formation by lenses. When two CCD cameras are used in this system, the detective angle can be expanded to ~~160° from~~ 10-170°. The angle resolution can reach 0.1° per pixel. The scattering signal from 0-10° and 170-180° cannot be detected, because the signal to noise ratio is significantly lower than the value needed to estimate the quantities effectively.

To decrease the total area of the instrument, the distance between the CCD cameras and the laser beam should be less than 1m.

So the ~~whole~~ CCD-LADS system ~~should~~ covers an area ~~of~~ 12m long and 1m wide. When the instrument is set up, the first step to do is to measure the relative position of the CCD cameras, the laser beam and the laser emitter. From the geometric relationship shown in ~~figure~~ Figure 1, we can know that the light scattered at different position on the laser beam will be collected by different pixels on the CCD, so that the scattering light at different angles can be retrieved from the image captured by CCD. Due to the open path structure of the CCD-LADS, the background noise is much higher in daytime than in ~~nighttime~~night time. Currently, the CCD-LADS system can just estimate the nocturnal aerosol scattering phase function.

2.2 Methodology

2.2.1 Data acquisition and pre-processing

The data acquisition of CCD-LADS is to obtain the angle-resolved scattering signals from images captured by two independent CCD systems, and then merge the signals ~~captured from two independent CCD-system, which can detect the scattering light from different scattering angles.~~ Firstly, the CCD-LADS is set up as shown in Figure 1(a). The geometric relationships among the CCDs, laser emitter and light trap are measured by tape. Then the scattering angle of laser in the image should be calibrated. The direction of the CCD cameras are adjusted to make sure that the image of laser go through the centre of the pixel arrays of CCD. By using a beam block the backscattering light is blocked from going into the CCD and the pixel related to the 90° scattering angle can be referred from the calibrated image (Figure 1(d)). Because of the equisolid projection is used by the lens, the distance from a point on the image on the CCD to the centre of the pixels can be calculated as $R = 2f \times \sin(\theta/2)$, where θ is the angle in rad between a point in the real world and the optical axis, which goes from the center of the image through the center of the lens, f is the focal length of the lens (Miyamoto, 1964). So the scattering angle, which is related to the centre of the image can be calculated by substituting the distance from the pixel related to the 90° scattering angle to the centre of pixels in the calibrated image into the equation of the equisolid projection. In this way, each pixel on the image of laser will be associated with a scattering angle. ~~The exposure time of these two CCDs should be in complete accord for the comparison.~~

At the beginning of the measurement, the CCDs are cooled down to -15°C to minimize the noise from dark current. Then a test image with a 10 s exposure time is captured to fix the exposure time of measurement by evaluating the signal intensity of this image. Generally, the maximum of the signal intensity is tuned to about 2^{14} because the limitation is 2^{16} . If the maximum increased to the limitation in an image, the exposure time will also be changed in the next image automatically. The exposure

time of these two CCDs that were always about 5-60 seconds in the past observations and should be in complete accordance for the comparison. After the test image, a dark frame image is captured for each CCD by using a shutter in front of the lens. The bias-dark current noise from the process and transmission of the signal can be subtracted during the procedure of image configuration by subtracting the dark frame image from the regular image (Figure 2(a)). The images are captured automatically after these steps.

Then a suitable exposure time is set to measure the scattering light. After image captured, the scattering light of the laser beam are separated from the background noise in the image as the follow steps. Firstly, the central axis of the scattering signals of laser beam from the scattering light is fitted in the program (the red line shown in Figure 2(b)). Then the signal-intensities of image y-of-the scattering-light-on the perpendicular of this central axis (the blue line shown in Figure 2(b)) are fitted with a normal distribution.

$$f(x) = I_0 + I \times \frac{1}{\sqrt{2\pi}\sigma} \exp\left(-\frac{(x-\mu)^2}{2\sigma^2}\right) \quad (1)$$

where I_0 is the intensity of the background noise, I is the intensity of the scattering signal of the laser beam related to one scattering angle, x represents the distance between the pixel on the perpendicular and on the central axis of the scattering signals, σ and μ are the fitting parameters of the normal distribution. Combining with the calibrated one-to-one correspondence between the image of laser and the scattering angle, the angle-resolved scattering signals is obtained from

different scattering angle is analysed to get the angle-resolved signal with the above steps of data acquisition.

When the angle-resolved signals from two CCDs are retrieved, the change of signals with angles can be merged by following the steps below. Firstly, the minimum angle θ_1 and maximum angle θ_2 of the overlap angular region of signals from two CCDs are set as the boundary angle of data merging (shadow zone in Figure 3). θ_1 and θ_2 are always around 50° and 80° , respectively. In this region, a transform coefficient with scattering angles $T(\theta)$ is calculated by using the overlap region of signals from two CCDs after quality control,

$$T(\theta) = \frac{I_1(\theta)}{I_2(\theta)} \quad (12)$$

$I_1(\theta)$ is the signal with the scattering angle θ captured by the first CCD while $I_2(\theta)$ is that of the second CCD. The transform coefficient T is an average of $T(\theta)$. The lifted signal $I_2'(\theta)$ can be calculated by multiplying $I_2(\theta)$ with the average of $T(\theta)$ (Figure 3). For the region where $\theta < \theta_1$ or $\theta > \theta_2$, scattering angles that just one CCD can captured,

the signal $I_1(\theta)$ or $I_2'(\theta)$ is used as the merged scattering signals $I(\theta)$ after merging, respectively. For the overlap region, a linear weighting average is done between $I_1(\theta)$ and $I_2'(\theta)$.

带格式的: 字体: 10 磅

带格式的: 字体: 10 磅

带格式的: 字体: 10 磅

带格式的: 字体: 10 磅

带格式的: 字体: 10 磅

带格式的: 字体: 10 磅

带格式的: 字体: 10 磅

带格式的: 字体: 10 磅

带格式的: 字体: 10 磅

带格式的: 字体: 10 磅

带格式的: 字体: 10 磅

带格式的: 字体: 10 磅

带格式的: 字体: 10 磅

带格式的: 字体: 10 磅

带格式的: 字体: 10 磅

带格式的: 字体: 10 磅

带格式的: 字体: (默认) Times New Roman, 10 磅, 非倾斜

带格式的: 字体: Times New Roman

$$I(\theta) = \begin{cases} I_1(\theta), & \theta < \theta_1 \\ \frac{\theta_2 - \theta}{\theta_2 - \theta_1} \times I_1(\theta) + \frac{\theta - \theta_1}{\theta_2 - \theta_1} \times I_2'(\theta), & \theta_1 \leq \theta \leq \theta_2 \\ I_2'(\theta), & \theta > \theta_2 \end{cases} \quad (3)$$

If the scattering angle is closer to the angle that just $I_1(\theta)$ can represent, the share of $I_1(\theta)$ is higher than $I_2'(\theta)$ and vice versa. Using the method above, the merged signals with scattering angles $I(\theta)$ can be estimated.

2.2.2 The retrieval algorithm to determine aerosol phase function

Figure 2 shows the flow chart of the retrieval algorithm to determine $p(\theta)$ from CCD-LADS measurements. According to the geometric structure of the CCD-LADS, the echo equation of CCD-LADS can be figured firstly,

$$I(\theta)E(\theta) = N_0\tau_Z\tau_R\beta(\theta) \quad (24)$$

where $E(\theta)$ is the received signals with scattering angles, $\beta(\theta)$ is the scattering function of atmospheric air molecules and

aerosols, τ_Z and τ_R are the transmittances on the optical paths of laser emitting and scattering respectively, N_0 is the calibration factor that depends on the optical efficiency of the transform-coefficient of the instrument. Depending on the area that the CCD-LADS covers, the longest distance between CCD cameras and the laser beam is less than 8m, the points on the laser beam is limited to less than 10m in the scattering range from 10° to 170° . In this range, an assumption that $\tau_Z = \tau_R = 1$ can be established with a threshold that the visibility should be larger than 1.5 km. The correlation between the visibility and extinction coefficient k_{ex} can be expressed as $k_{ex} = 3/\text{visibility}(km)$ (Chen et al., 2012) which means that the assumption can be established if k_{ex} is smaller than 2 km^{-1} . In some extreme pollution processes with high concentrations of both aerosol and gaseous pollutants (Ma et al., 2011; Xu et al., 2011), the scattering and absorption of aerosols and gases (NO_2 (Dixon, 1940), O_3 (Burrows et al., 1999), etc.) may lead to extreme k_{ex} values. If the k_{ex} is more than 2 km^{-1} , the assumption cannot be applied while the transmittance can be calculated with the measurement of visibility. With the assumption, and equation (24)

can be transformed to $I(\theta)E(\theta) = N_0\beta(\theta)$.

Aerosol Scattering phase function $p(\theta)$ is the normalized angular distribution of the scattering function,

$$p(\theta) = \frac{4\pi\beta(\theta)}{\int_0^{180} \beta(\theta)d\theta} = \frac{4\pi I(\theta)}{\int_0^{180} I(\theta)d\theta} \quad (5)$$

So the scattering phase function can be calculated directly from $I(\theta)$ measured by CCD-LADS. If the scattering function of aerosols $\beta_{aero}(\theta)$ is known, the $p(\theta)$ can be calculated. Therefore, a retrieval algorithm is built to separate the scattering signals with angles into the scattering of aerosols and air molecules (shown in the dashed box in Figure 4).

As the first step, the scattering coefficient of air molecules at near surface level k_{sc-air} is calculated with the density of atmosphere, which depends on the surface pressure and temperature by a Rayleigh scattering model,

$$k_{sc-air} = \frac{8\pi^3(m^2-1)^2}{3n_{air}\lambda^4} \quad (36)$$

带格式的: 字体: Times New Roman

带格式的: 下标

带格式的: 下标

带格式的: 缩进: 左侧: 0 厘米, 首行缩进: 0 厘米

带格式的: 字体: 非倾斜

带格式的: 字体: Times New Roman

带格式的: 字体: Times New Roman

带格式的: 字体: Times New Roman, 非倾斜

带格式的: 字体: (默认) Cambria Math, (中文) Times New Roman

带格式的: 字体: (中文) + 中文正文 (宋体), (中文) 中文 (中国)

带格式的: 字体: (中文) + 中文正文 (宋体), (中文) 中文 (中国)

带格式的: 字体: 10 磅

where n_{air} is the number density of air molecules, which depends on the surface pressure and temperature measured by the weather station, m is the index of refraction of atmosphere, which depends on n_{air} and the wavelength of the laser λ . The hemispheric backscattering coefficient of air molecules $k_{bsc-air}$ is a half of k_{sc-air} (Bohren and Huffman, 2008).

To resolve the ratio between the air molecules and the total aerosol hemispheric scattering $R_{air} = \frac{k_{bsc-air}}{k_{bsc-air} + k_{bsc-aero}}$, the

5 scattering coefficient of aerosols $k_{sc-aero}$ and the hemispheric backscattering coefficient of aerosols $k_{bsc-aero}$ are measured with an integrating nephelometer here.

To solve the intensity of the total hemispheric backscattering scattering signals I_{bsc} , the angle-resolved scattering signals should be integrated from 90° to 180° scattering angle. Because of the detective angular range of CCD-LADS is 10° - 170° , the angular truncation correction is necessary to resolve the hemispheric scattering intensity. For the backward angular

10 truncation, the scattering intensity in that range is assumed to be equal to the scattering intensity at the largest scattering angle that CCD-LADS can measured. After the correction above, the corrected intensity $I'(\theta)$ is used to obtain I_{bsc} .

$$I_{bsc} = \int_0^{2\pi} \int_{\pi/2}^{\pi} I'(\theta) \sin \theta d\theta d\varphi \quad (7)$$

Then the angle-resolved scattering signals of air molecules can be calculated with a molecular phase function (Bohren and Huffman, 2008), normalized parameter of air molecules scatter N_1 and N_2 can be calculated with k_{sc-air} , $k_{sc-aero}$, $k_{bsc-air}$

15 and $k_{bsc-aero}$,

$$N_1 = \frac{\int_0^{2\pi} \int_0^{\pi} E(\theta) \sin \theta d\theta d\varphi \times \frac{k_{sc-air}}{k_{sc-air} + k_{sc-aero}}}{4\pi} \quad (4)$$

$$N_2 I_{air}(\theta) = \frac{3(1 + \cos^2 \theta)}{4} \times \frac{I_{bsc} \int_0^{2\pi} \int_{\pi/2}^{\pi} E(\theta) \sin \theta d\theta d\varphi \times R_{air} \frac{k_{bsc-air}}{k_{bsc-air} + k_{bsc-aero}}}{2\pi} \quad (5)$$

where N_1 and N_2 are the calculated angle-resolved scattering signals of air molecules. According to

20 equation (4), the aerosol phase function $p_{aero}(\theta)$ can be estimated as,

$$p_{aero}(\theta) = \frac{4\pi(I(\theta) - I_{air}(\theta))}{\int_0^{180} (I(\theta) - I_{air}(\theta)) d\theta}$$

(9) with the total scattering coefficient and the hemispheric backscattering coefficient separately. The received scattering signals are integrated on the spherical surface, and then multiplied by the percentage of air scattering to get these parameters.

The physical significance of these parameters is to indicate the intensity of air scatter.

25 Because of the detective angular range of CCD-LADS is 10° - 170° degree, the angular truncation correction is necessary to resolve the total scattering intensity. For the forward angular truncation, several aerosol phase functions proposed in the previous studies are used to calculate the correlation coefficient with the signal profile, and then the one with a best correlation is chosen to fit the signal profile in this angular range. For the backward angular truncation, the scattering intensity in that range is assumed to be equal to the scattering intensity at the largest scattering angle that CCD-LADS can measured. After the

30 correction above, the corrected intensity $E'(\theta)$ is used in equation (4) and (5) to resolve the N_1 and N_2 .

带格式的: 字体: Times New Roman

带格式的: 字体: Times New Roman

带格式的: 字体: Times New Roman

带格式的: 字体: (默认) Cambria Math, (中文) Times New Roman

If the difference between N_1 and N_2 is less than 10% in the test, the result will be accepted. Combine the normalized parameter, air scattering phase function and $E^i(\theta)$, the scattering intensities of aerosols with scattering angles ($E_{aero}(\theta)$) can be calculated,

$$E_{aero}(\theta) = E^i(\theta) - \frac{3(1+\cos^2\theta)}{4} \times \frac{N_1+N_2}{2} \quad (6)$$

5 Because the $p(\theta)$ is a normalized function and directly proportional to $E_{aero}(\theta)$, it can be normalized with $E_{aero}(\theta)$.

2.2.3 Error analysis

Two types of uncertainties determine the error of the retrieved aerosol phase function: the measurement errors caused by the processes of obtaining the angle-resolved signals, and an error introduced by the retrieval algorithm.

10 There are two sources of measurement errors in the data acquisition processes introduced in Section 2.2.1. Firstly, the measurement error of CCD used in the CCD-LADS is 10% according to the related manual. The relative difference between the fitted normal distribution introduced in equation (1) and the measured signal in the laboratory study is 8.8% \pm 1.5%, which can also certify the 10% measuring error on I introduced by the manual of CCD. Secondly, the measurement of the geometric relationship will lead to at most 5% relative error on the scattering angle θ introduced by the resolution and accuracy of the used tools.

15 The relative errors on the merged angle-resolved signals $I(\theta)$ can be derived by applying a standard propagation of errors to equation (3) (Bevington and Robinson, 2003),

$$\left(\frac{\Delta I}{I}\right)^2 = F_{I_1} \left(\frac{\Delta I_1}{I_1}\right)^2 + F_{I_2} \left(\frac{\Delta I_2}{I_2}\right)^2 + F_{\theta} \left(\frac{\Delta \theta}{\theta}\right)^2 \quad (10)$$

where σ symbol means the standard deviation of variables, $\frac{\Delta x}{x}$ is equal to the relative error of x and the propagation factor

20 F_x are defined as $F_x = \left(\frac{x}{I} \frac{\partial I}{\partial x}\right)^2$. By substituting the relative errors and the average signals into equation (10), the uncertainties on $I(\theta)$ are calculated as a distribution with angular shown in Figure 5. The values of uncertainties on $I(\theta)$ are between 10% and 19%, and varied with angles.

The uncertainties of the retrieval algorithm are introduced by the uncertainties of the input parameters. There are three groups of input parameters in the retrieval algorithm: merged angle-resolved signals, aerosol hemi-backscattering coefficient and temperature/pressure. The errors of the temperature and pressure are about 0.1 K and 0.1 hPa (Box and Steffen, 2001), respectively, which will lead to a 0.02% uncertainty on $k_{bsc-air}$. Combined the 10% uncertainties on the measured $k_{bsc-aero}$ (Heintzenberg et al., 2006), the uncertainty of R_{air} can be calculated as 7% with the algorithm in Section 2.2.2. According to the algorithm shown in Figure 4, the uncertainty of the retrieved aerosol phase function are mainly dominated by the uncertainties of the merged signal shown in Figure 5, and also influenced by the uncertainty of R_{air} in a way.

带格式的：标题 3，段落间距段前：12 磅，段后：12 磅，行距：单倍行距

带格式的：字体：Times New Roman

带格式的：德语(德国)

带格式的：德语(德国)

带格式的：字体：Times New Roman

带格式的：字体：(中文)+中文正文(宋体)，英语(美国)

3 Results

3.1 Laboratory Results

To validate the ability of the CCD-LADS to measure the aerosol phase function, an indoor experiment was held in the laboratory in the Physics Building at Peking University during November 7-8th, 2015. The time resolution of CCD-LADS was set to 60 s during the experiment, while the angular detection ranged from 10 to 170°. The aerosol scattering coefficient, number size distribution, mass concentration of black carbon particles, ambient temperature and relative humidity were measured with an integrating nephelometer (Model 3563, TSI, Inc., Shoreview, MN, USA), a scanned mobility particle sizer (SMPS; Model 3936, TSI, Inc., Shoreview, MN, USA), an aerodynamic particle sizer (APS; Model 3321, TSI, Inc., Shoreview, MN, USA), a micro-aethalometer (Model AE51, Magee Scientific, Berkeley, CA, USA) and a dew-point chilled mirror sensor (Edgetech DewMaster), respectively.

Figure 3-6 shows the time series of several quantities during the laboratory experiment. The scattering/hemispheric backscattering coefficient of aerosols at 525 nm wavelength shown in Figure 3-6(b) and the mass concentration of black carbon particles shown in Figure 6-3(c) reveal the same pattern that first declines and climbs up afterwards. The same pattern can be discovered in the time series of particle number size distributions shown in Figure 6-3(d). The variation reflects the slow exchange between the air indoor and outdoor. The peak diameter of aerosol number size distribution was still around 100 nm, while it had a slight shift during the experiment. Therefore, the fine particles are dominant in the laboratory. The single scattering albedo (SSA) shown in Figure 6-3(c) was around 0.85 which means that the black carbon aerosol took up a relatively large proportion among the aerosol species, resulting in strong particle light absorption ability.

Combining the particle number size distributions measured with SMPS/APS and the mass concentration of black carbon aerosols measured with AE51 (Figure 6) into a modified Mie-scattering model, the aerosol optical properties including the aerosol phase function could be modelled (Ma et al., 2011). In this study (both laboratory and field study), the refractive index used for black carbon component is 1.95-0.79i (Seinfeld and Pandis, 2006), and for non-absorbing component is 1.53-10⁻⁷i (Wex et al., 2002). The mass ratio between two different mixing states (external or core-shell, which are two different ways black carbon and non-absorbing aerosols are mixed) of black carbon aerosols is assumed to be 1:1 according to the result of Ma et al. (2012). Figure 4-7 shows the comparison among the aerosol phase functions retrieved with the CCD-LADS retrieval algorithm, modelled with the modified Mie model and offered by the aerosol classification from the Cloud-Aerosol Lidar and Infrared Pathfinder Satellite Observations (CALIPSO) aerosol products (Omar et al., 2009). The CALIPSO aerosol classifications are based on the cluster analysis of the Aerosol Robotic Network (AERONET) measurements to determine characteristic aerosol types (Omar et al., 2005). Here the red solid line shows the retrieved $p(\theta)$ from the CCD-LADS measurements with the retrieval algorithm introduced in Sect. 2.2.2, while the brown dashed line shows the retrieved $p(\theta)$ from CCD-LADS directly without considering the air molecules scattering influence. The blue dashed line shows the modelled

result, and the other dotted lines express the aerosol phase functions of different aerosol types from CALIPSO aerosol classification. The uncertainty of the retrieved $p(\theta)$ and simulated $p(\theta)$ with Mie model, which is about 30% (Ma et al., 2011), are shown as error bars. The result shows that the comparison between the modelled $p(\theta)$ and the $p(\theta)$ retrieved with the retrieval algorithm shows a better agreement than the comparison between the modelled $p(\theta)$ and the $p(\theta)$ retrieved from the CCD-LADS measurements directly, especially for the backward scattering. The reason of this phenomenon is that the scattering coefficients of aerosols and air molecules are closer to each other for the backward scatter than for the forward scatter based on the background that the total scattering coefficient of aerosols is always much higher than that of air molecules. The comparison also shows that the retrieved $p(\theta)$ is closer to the aerosol phase function of the “biomass burning” aerosol among the several aerosol types classified from CALIPSO aerosol products. Compared with the other aerosol types, the “biomass burning” aerosol represents a better absorption ability due to the larger percentage of black carbon aerosol and organic aerosol, and also a smaller effective diameter around 100 nm (Omar et al., 2005; Rissler et al., 2006; Zhu et al., 2017) which is lower than 100 nm. The SSA and particle number size distribution of aerosols during the experiment shown in Figure 6 also have the similar characteristics with the “biomass burning” aerosol.

To further validate the quality of the retrieved result from the CCD-LADS measurement, a comparison was also carried out among the $p(\theta)$ at 42° scattering angle resolved with different methods (Figure 58). The $p(\theta)$ at 42° scattering angle is relatively typical and comparable because 42° is the scattering angle used in the forward scattering visibility sensor (Kessner et al., 2013). The result of the comparison shows that the $p(\theta)$ from CCD-LADS measurement and Mie model have the same pattern and the average difference in the absolute values between these two $p(\theta)$ is less than 10% not obvious.

3.2 Field Measurements

During January 2016, a comprehensive field campaign focused on air pollution in winter was conducted at the roof of a school building in Yanqi campus of the University of Chinese Academy of sciences (UCAS) in Huairou district, Beijing (40°24' N, 116°40' E, 94-91 m a.s.l.). The observatory is 60-60 km away from the downtown of Beijing and is at the edge of the North China Plain (NCP), which makes it suitable for measuring the regional pollution properties of the NCP (Ma et al., 2016).

During the campaign, all the instruments except for the CCD-LADS were housed in a laboratory with a steady room temperature as 20-20°C. The aerosols were sampled from an inlet 5 m higher than the ground and then dried to a relative humidity less than 30% before flowing into the laboratory to measure the aerosol number size distribution, scattering coefficient, phase function and the mass concentration of black carbon aerosols at a dry condition. The CCD-LADS was mounted outside the laboratory at the same altitude to measure the scattering phase function of ambient aerosols. Depending on the limitation of the ambient condition, the angular detection range of the CCD-LADS was 30-160° in this campaign.

带格式的: 字体: (默认) Times New Roman, (中文)
Times New Roman

带格式的: 字体: (中文) Times New Roman, 10 磅

带格式的: 字体: (默认) Times New Roman, (中文)
Times New Roman

带格式的: 字体: (默认) Times New Roman, (中文)
Times New Roman

带格式的: 字体: (默认) Times New Roman, (中文)
Times New Roman

带格式的: 字体: (默认) Times New Roman, (中文)
Times New Roman

带格式的: 字体: (默认) Times New Roman, (中文)
Times New Roman

带格式的: 字体: Times New Roman

带格式的: 字体: Times New Roman

During the field measurement, the scattering phase function of dry aerosols could be resolved from two ways: Aurora 4000 polar nephelometer measurements and the modified Mie-scattering model with the related aerosol measurements. Under high relative humidity condition, aerosol particles will absorb moisture in the atmosphere and exhibit hygroscopic growth, grow up significantly (Bian et al., 2014; Chen et al., 2014; Kuang et al., 2016a), and hence the scattering properties of ambient and dry aerosols are totally different. Therefore, the data collected at a relative humidity above 70% were kicked-off-eliminated from the comparison among the scattering phase functions of dry and ambient aerosols obtained by different methods. Figure 6-9 shows the result of the comparison mentioned above. The results from three methods are consistent with one another in the overlap of the detectable scattering angular range. Compared with the other results, the retrieval of CCD-LADS measurement enhances the backward scattering fraction of aerosol. This might be caused by the angular range (30-160°), which did not reach 10-170° and therefore might have increased errors in retrieving the angular distribution of aerosol scattering. The $p(\theta)$ from Aurora 4000 measurements have the similar average pattern with the results from other methods, but the deviation of its pattern is also obvious. Compared to the Aurora 4000 results, there are two significant advantages of CCD-LADS: wider detection range and better stability.

4 Discussions and Conclusions

A novel instrument named charge-coupled device-laser aerosol detective system (CCD-LADS) was developed to measure the nocturnal ambient aerosol phase function in the ambient atmosphere at a wider range of detection angles and a higher accuracy. The validation in both laboratory and field measurement shows the ability of CCD-LADS to measure the aerosol phase function. A laser is emitted horizontally, while two CCD cameras with fisheye lenses are installed besides the laser beam at the same altitude to capture the scattering signal from the laser beam with the cameras facing forward and backward, respectively. Then the signal captured by the two cameras are merged into one signal curve. The detectable angular range is from 10-170°, while the angle resolution reach 0.1° per pixel. A retrieval algorithm is developed to subtract the influence of air molecules scattering with the integrating nephelometer and weather station measurements. The uncertainties of CCD-LADS were discussed. To validate the ability of CCD-LADS to measure the aerosol phase function, an indoor experiment was held in the laboratory of the Physics Building at Peking University during November 7-8th, 2015. During the experiment, the angular detection range was from 10-170°. The comparison between the modelled $p(\theta)$ and the retrieved $p(\theta)$ shows an excellent agreement. Both of them are close to the aerosol phase function of the “biomass burning” aerosol from CALIPSO aerosol products. The comparison result is reasonable, because the SSA and particle number size distribution of aerosols during the experiment also had similar characteristics with the “biomass burning” aerosol. The comparison of the $p(\theta)$ at 42° scattering angle acquired by different methods also shows good agreements on both patterns and absolute values.

During January 2016, a comprehensive field campaign focused on air pollution in winter was organized at the roof of a school building in Yanqi campus of the UCAS. Depending on the limitation of ambient condition, the angular detection range of the CCD-LADS was 30-160° in this campaign. The retrieved aerosol phase function with CCD-LADS measurements is consistent with both the Aurora 4000 measurement and the modified Mie model results in the overlap region of the detectable scattering angular range. Compared with the Aurora 4000 measurements during this campaign, the CCD-LADS measurements are steadier.

Both the laboratory experiment and the field measurement have demonstrated that the CCD-LADS is a robust instrument, fully capable of measuring the ambient aerosol phase function under different conditions. Overall, compared with the laboratory-scale instruments, the CCD-LADS measured aerosol phase functions in a wider angular range and a higher angular resolution.

10 Acknowledgements

This work is supported by the National Natural Science Foundation of China (41590872, 41375134).

References

- [Barkey, B., Bailey, M., Liou, K.-N., and Hallett, J.: Light-scattering properties of plate and column ice crystals generated in a laboratory cold chamber, *Applied Optics*, 41, 5792-5796, 2002.](#)
- 15 [Anderson, T. L., Covert, D. S., Marshall, S. F., Laucks, M. L., Charlson, R. J., Waggoner, A. P., Ogren, J. A., Caldow, R., Holm, R. L., Quant, F. R., Sem, G. J., Wiedensohler, A., Ahlquist, N. A., and Bates, T. S.: Performance Characteristics of a High-Sensitivity, Three-Wavelength, Total Scatter/Backscatter Nephelometer, *Journal of Atmospheric and Oceanic Technology*, 13, 967-986, 10.1175/1520-0426\(1996\)013<0967:PCOAHS>2.0.CO;2, 1996.](#)
- [Andrews, E., Sheridan, P. J., Fiebig, M., McComiskey, A., Ogren, J. A., Arnott, P., Covert, D., Elleman, R., Gasparini, R.,](#)
- 20 [Collins, D., Jonsson, H., Schmid, B., and Wang, J.: Comparison of methods for deriving aerosol asymmetry parameter, *Journal of Geophysical Research: Atmospheres*, 111, n/a-n/a, 10.1029/2004JD005734, 2006.](#)
- [Barkey, B., Bailey, M., Liou, K.-N., and Hallett, J.: Light-scattering properties of plate and column ice crystals generated in a laboratory cold chamber, *Applied Optics*, 41, 5792-5796, 2002.](#)
- [Barkey, B., Paulson, S. E., and Chung, A.: Genetic Algorithm Inversion of Dual Polarization Polar Nephelometer Data to Determine Aerosol Refractive Index, *Aerosol Science and Technology*, 41, 751-760, 2007.](#)
- 25 [Bevington, P. R., and Robinson, D. K.: Data reduction and error analysis, Third ed., Physical Science - Astronomy, McGraw-Hill Education, 336 pp., 2003.](#)
- [Bian, Y. X., Zhao, C. S., Ma, N., Chen, J., and Xu, W. Y.: A study of aerosol liquid water content based on hygroscopicity measurements at high relative humidity in the North China Plain, *Atmos. Chem. Phys.*, 14, 6417-6426, 2014.](#)

- Bohren, C. F., and Huffman, D. R.: Absorption and scattering of light by small particles, John Wiley & Sons, 2008.
- Box, J. E., and Steffen, K.: Sublimation on the Greenland Ice Sheet from automated weather station observations, *Journal of Geophysical Research: Atmospheres*, 106, 33965-33981, 10.1029/2001jd900219, 2001.
- Burrows, J. P., Richter, A., Dehn, A., Deters, B., Himmelmann, S., Voigt, S., and Orphal, J.: ATMOSPHERIC REMOTE-
5 SENSING REFERENCE DATA FROM GOME—2. TEMPERATURE-DEPENDENT ABSORPTION CROSS SECTIONS
OF O₃ IN THE 231–794NM RANGE, *Journal of Quantitative Spectroscopy and Radiative Transfer*, 61, 509-517,
[http://dx.doi.org/10.1016/S0022-4073\(98\)00037-5](http://dx.doi.org/10.1016/S0022-4073(98)00037-5), 1999.
- Castagner, J.-L. and Bigio, I. J.: Particle sizing with a fast polar nephelometer, *Applied Optics*, 46, 527-532, 2007.
- Castagner, J.-L. and Bigio, I. J.: Polar nephelometer based on a rotational confocal imaging setup, *Applied Optics*, 45, 2232-
10 2239, 2006.
- Chen, J., Zhao, C. S., Ma, N., Liu, P. F., Göbel, T., Hallbauer, E., Deng, Z. Z., Ran, L., Xu, W. Y., Liang, Z., Liu, H. J., Yan,
P., Zhou, X. J., and Wiedensohler, A.: A parameterization of low visibilities for hazy days in the North China Plain, *Atmos.
Chem. Phys.*, 12, 4935-4950, 10.5194/acp-12-4935-2012, 2012.
- Chen, J., Zhao, C. S., Ma, N., and Yan, P.: Aerosol hygroscopicity parameter derived from the light scattering enhancement
15 factor measurements in the North China Plain, *Atmos. Chem. Phys.*, 14, 8105-8118, 2014.
- Curtis, D. B., Aycibin, M., Young, M. A., Grassian, V. H., and Kleiber, P. D.: Simultaneous measurement of light-scattering
properties and particle size distribution for aerosols: Application to ammonium sulfate and quartz aerosol particles,
Atmospheric Environment, 41, 4748-4758, 2007.
- Curtis, D. B., Meland, B., Aycibin, M., Arnold, N. P., Grassian, V. H., Young, M. A., and Kleiber, P. D.: A laboratory
20 investigation of light scattering from representative components of mineral dust aerosol at a wavelength of 550 nm, *Journal of
Geophysical Research: Atmospheres*, 113, D08210, 2008.
- Dixon, J. K.: The Absorption Coefficient of Nitrogen Dioxide in the Visible Spectrum, *The Journal of Chemical Physics*, 8,
157-160, 10.1063/1.1750622, 1940.
- Draine, B. T. and Flatau, P. J.: Discrete-Dipole Approximation For Scattering Calculations, *Journal of the Optical Society of
25 America A*, 11, 1491-1499, 1994.
- Heintzenberg, J., and Charlson, R. J.: Design and Applications of the Integrating Nephelometer: A Review, *Journal of
Atmospheric and Oceanic Technology*, 13, 987-1000, 10.1175/1520-0426(1996)013<0987:DAAOTI>2.0.CO;2, 1996.
- Heintzenberg, J., Wiedensohler, A., Tuch, T. M., Covert, D. S., Sheridan, P., Ogren, J. A., Gras, J., Nessler, R., Kleefeld, C.,
Kalivitis, N., Aaltonen, V., Wilhelm, R.-T., and Havlicek, M.: Intercomparisons and Aerosol Calibrations of 12 Commercial
30 Integrating Nephelometers of Three Manufacturers, *Journal of Atmospheric and Oceanic Technology*, 23, 902-914,
10.1175/jtech1892.1, 2006.
- Hulst, H. C. v. d.: Light scattering by small particles, Dover Publications, 1957.

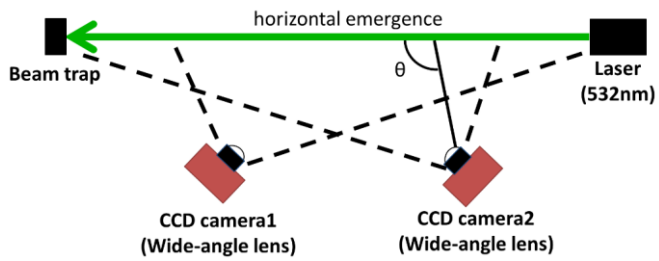
- Kessner, A. L., Wang, J., Levy, R. C., and Colarco, P. R.: Remote sensing of surface visibility from space: A look at the United States East Coast, *Atmospheric Environment*, 81, 136-147, 2013.
- Kim, H., Barkey, B., and Paulson, S. E.: Real refractive indices of α - and β -pinene and toluene secondary organic aerosols generated from ozonolysis and photo-oxidation, *Journal of Geophysical Research: Atmospheres*, 115, D24212, 2010.
- 5 Kuang, Y., Zhao, C. S., Ma, N., Liu, H. J., Bian, Y. X., Tao, J. C., and Hu, M.: Deliquescent phenomena of ambient aerosols on the North China Plain, *Geophysical Research Letters*, 43, 8744-8750, 2016a.
- Kuang, Y., Zhao, C. S., Tao, J. C., Bian, Y. X., and Ma, N.: Impact of aerosol hygroscopic growth on the direct aerosol radiative effect in summer on North China Plain, *Atmospheric Environment*, 147, 224-233, 2016b.
- Kuang, Y., Zhao, C. S., Tao, J. C., and Ma, N.: Diurnal variations of aerosol optical properties in the North China Plain and
10 their influences on the estimates of direct aerosol radiative effect, *Atmos. Chem. Phys.*, 15, 5761-5772, 2015.
- Ma, N., Zhao, C., Tao, J., Wu, Z., Kecorius, S., Wang, Z., Größ, J., Liu, H., Bian, Y., Kuang, Y., Teich, M., Spindler, G., Müller, K., van Pinxteren, D., Herrmann, H., Hu, M., and Wiedensohler, A.: Variation of CCN activity during new particle formation events in the North China Plain, *Atmos. Chem. Phys.*, 16, 8593-8607, 2016.
- Ma, N., Zhao, C. S., Müller, T., Cheng, Y. F., Liu, P. F., Deng, Z. Z., Xu, W. Y., Ran, L., Nekat, B., van Pinxteren, D., Gnauk,
15 T., Müller, K., Herrmann, H., Yan, P., Zhou, X. J., and Wiedensohler, A.: A new method to determine the mixing state of light absorbing carbonaceous using the measured aerosol optical properties and number size distributions, *Atmos. Chem. Phys.*, 12, 2381-2397, 2012.
- Ma, N., Zhao, C. S., Nowak, A., Müller, T., Pfeifer, S., Cheng, Y. F., Deng, Z. Z., Liu, P. F., Xu, W. Y., Ran, L., Yan, P., Göbel, T., Hallbauer, E., Mildenberger, K., Henning, S., Yu, J., Chen, L. L., Zhou, X. J., Stratmann, F., and Wiedensohler, A.:
20 Aerosol optical properties in the North China Plain during HaChi campaign: an in-situ optical closure study, *Atmos. Chem. Phys.*, 11, 5959-5973, 2011.
- McCrowey, C. J., Tinilau, S. S., Calderon, G., Koo, J.-E., and Curtis, D. B.: A Portable High-Resolution Polar Nephelometer for Measurement of the Angular Scattering Properties of Atmospheric Aerosol: Design and Validation, *Aerosol Science and Technology*, 47, 592-605, 2013.
- 25 Mishchenko, M. I., Travis, L. D., and Mackowski, D. W.: T-matrix computations of light scattering by nonspherical particles: A review, *Journal of Quantitative Spectroscopy and Radiative Transfer*, 55, 535-575, 1996.
- [Müller, T., Laborde, M., Kassell, G., and Wiedensohler, A.: Design and performance of a three-wavelength LED-based total scatter and backscatter integrating nephelometer, *Atmos. Meas. Tech.*, 4, 1291-1303, 10.5194/amt-4-1291-2011, 2011.](#)
- [Muñoz, O., Volten, H., de Haan, J. F., Vassen, W., and Hovenier, J. W.: Experimental determination of scattering matrices of
30 randomly oriented fly ash and clay particles at 442 and 633 nm, *Journal of Geophysical Research: Atmospheres*, 106, 22833-22844, 10.1029/2000JD000164, 2001.](#)

- Muñoz, O., Volten, H., de Haan, J. F., Vassen, W., and Hovenier, J. W.: Experimental determination of the phase function and degree of linear polarization of El Chichón and Pinatubo volcanic ashes, *Journal of Geophysical Research: Atmospheres*, 107, ACL 4-1-ACL 4-8, 10.1029/2001JD000983, 2002.
- Muñoz, O., Moreno, F., Guirado, D., Ramos, J. L., López, A., Girela, F., Jerónimo, J. M., Costillo, L. P., and Bustamante, I.: Experimental determination of scattering matrices of dust particles at visible wavelengths: The IAA light scattering apparatus, *Journal of Quantitative Spectroscopy and Radiative Transfer*, 111, 187-196, <http://dx.doi.org/10.1016/j.jqsrt.2009.06.011>, 2010.
- Muñoz, O., and Hovenier, J. W.: Laboratory measurements of single light scattering by ensembles of randomly oriented small irregular particles in air. A review, *Journal of Quantitative Spectroscopy and Radiative Transfer*, 112, 1646-1657, <http://dx.doi.org/10.1016/j.jqsrt.2011.02.005>, 2011.
- Omar, A. H., Won, J.-G., Winker, D. M., Yoon, S.-C., Dubovik, O., and McCormick, M. P.: Development of global aerosol models using cluster analysis of Aerosol Robotic Network (AERONET) measurements, *Journal of Geophysical Research: Atmospheres*, 110, D10S14, 10.1029/2004JD004874, 2005.
- Muñoz, O. and Hovenier, J. W.: Laboratory measurements of single light scattering by ensembles of randomly oriented small irregular particles in air. A review, *Journal of Quantitative Spectroscopy and Radiative Transfer*, 112, 1646-1657, 2011.
- Muñoz, O., Moreno, F., Guirado, D., Ramos, J. L., López, A., Girela, F., Jerónimo, J. M., Costillo, L. P., and Bustamante, I.: Experimental determination of scattering matrices of dust particles at visible wavelengths: The IAA light scattering apparatus, *Journal of Quantitative Spectroscopy and Radiative Transfer*, 111, 187-196, 2010.
- Muñoz, O., Volten, H., de Haan, J. F., Vassen, W., and Hovenier, J. W.: Experimental determination of scattering matrices of randomly oriented fly ash and clay particles at 442 and 633 nm, *Journal of Geophysical Research: Atmospheres*, 106, 22833-22844, 2001.
- Omar, A. H., Winker, D. M., Vaughan, M. A., Hu, Y., Trepte, C. R., Ferrare, R. A., Lee, K.-P., Hostetler, C. A., Kittaka, C., Rogers, R. R., Kuehn, R. E., and Liu, Z.: The CALIPSO Automated Aerosol Classification and Lidar Ratio Selection Algorithm, *Journal of Atmospheric and Oceanic Technology*, 26, 1994-2014, 2009.
- Pachauri, R. K., Allen, M. R., Barros, V. R., Broome, J., Cramer, W., Christ, R., Church, J. A., Clarke, L., Dahe, Q., Dasgupta, P., Dubash, N. K., Edenhofer, O., Elgizouli, I., Field, C. B., Forster, P., Friedlingstein, P., Fuglestad, J., Gomez-Echeverri, L., Hallegatte, S., Hegerl, G., Howden, M., Jiang, K., Jimenez Cisneros, B., Kattsov, V., Lee, H., Mach, K. J., Marotzke, J., Mastrandrea, M. D., Meyer, L., Minx, J., Mulugetta, Y., O'Brien, K., Oppenheimer, M., Pereira, J. J., Pichs-Madruga, R., Plattner, G.-K., Pörtner, H.-O., Power, S. B., Preston, B., Ravindranath, N. H., Reisinger, A., Riahi, K., Rusticucci, M., Scholes, R., Seyboth, K., Sokona, Y., Stavins, R., Stocker, T. F., Tschakert, P., van Vuuren, D., and van Ypersele, J.-P.: *Climate Change*

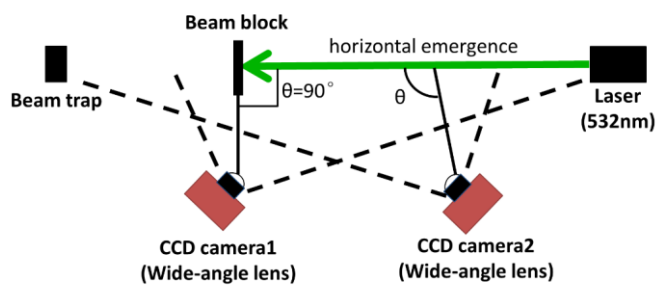
- 2014: Synthesis Report. Contribution of Working Groups I, II and III to the Fifth Assessment Report of the Intergovernmental Panel on Climate Change, edited by: Pachauri, R. K., and Meyer, L., IPCC, Geneva, Switzerland, 151 pp., 2014.
- Rissler, J., Vestin, A., Swietlicki, E., Fisch, G., Zhou, J., Artaxo, P., and Andreae, M. O.: Size distribution and hygroscopic properties of aerosol particles from dry-season biomass burning in Amazonia, *Atmos. Chem. Phys.*, 6, 471-491, 10.5194/acp-6-471-2006, 2006.
- Seinfeld, J. H., and Pandis, S. N.: *Atmospheric Chemistry and Physics*, Second ed., John Wiley & Sons, 2006.
- Tao, J. C., Zhao, C. S., Ma, N., and Liu, P. F.: The impact of aerosol hygroscopic growth on the single-scattering albedo and its application on the NO₂ photolysis rate coefficient, *Atmos. Chem. Phys.*, 14, 12055-12067, 2014.
- Wex, H., Neusüß, C., Wendisch, M., Stratmann, F., Koziar, C., Keil, A., Wiedensohler, A., and Ebert, M.: Particle scattering, backscattering, and absorption coefficients: An in situ closure and sensitivity study, *Journal of Geophysical Research: Atmospheres*, 107, LAC 4-1-LAC 4-18, 10.1029/2000JD000234, 2002.
- Xu, W. Y., Zhao, C. S., Ran, L., Deng, Z. Z., Liu, P. F., Ma, N., Lin, W. L., Xu, X. B., Yan, P., He, X., Yu, J., Liang, W. D., and Chen, L. L.: Characteristics of pollutants and their correlation to meteorological conditions at a suburban site in the North China Plain, *Atmos. Chem. Phys.*, 11, 4353-4369, 10.5194/acp-11-4353-2011, 2011.
- Zhu, J., Xia, X., Wang, J., Zhang, J., Wiedinmyer, C., Fisher, J. A., and Keller, C.: Impact of Southeast Asian smoke on aerosol properties in Southwest China: first comparison of model simulations with satellite and ground observations, *Journal of Geophysical Research: Atmospheres*, 2016JD025793, 10.1002/2016jd025793, 2017.

带格式的: 居中

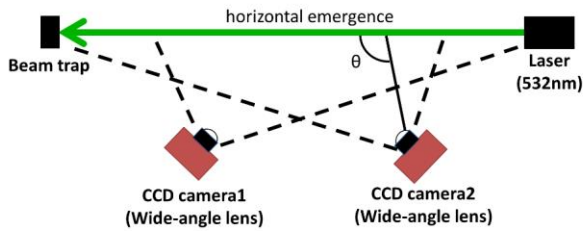
(a) Measurement setup



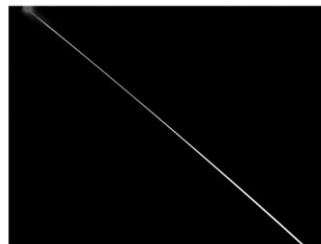
(b) Calibration setup



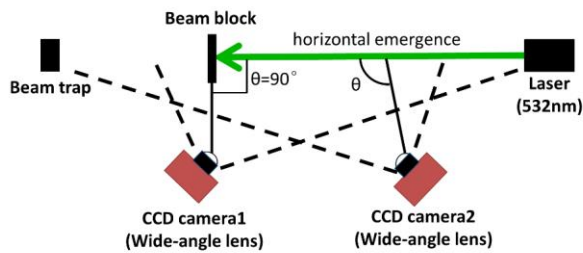
(a) Measurement setup



(c) Measured image



(b) Calibration setup



(d) Calibrated image

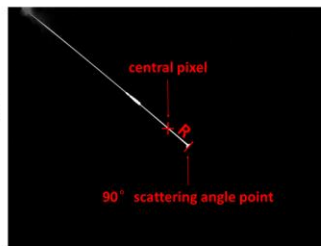


Figure 1: Sketch map of the geometric relationship and the sampling image of CCD-LADS

(a) Dark current noise subtraction



(b) Background noise subtraction

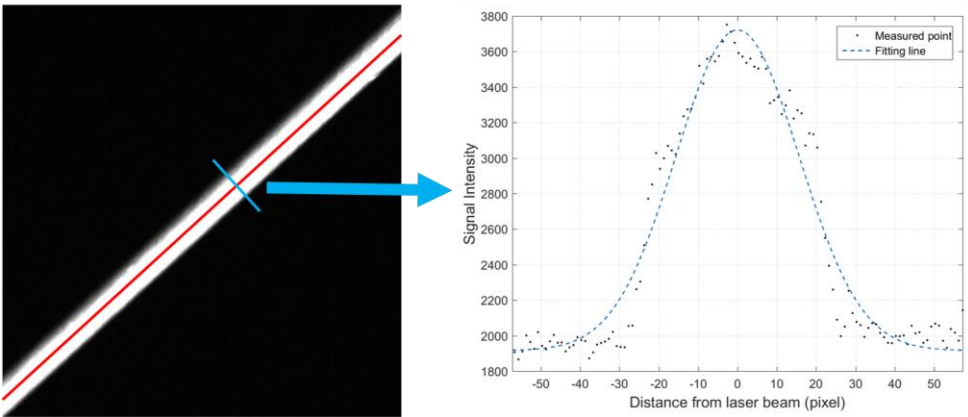


Figure 2: Noise subtraction of CCD-LADS: (a) Dark current noise subtraction; (b) Background noise subtraction.

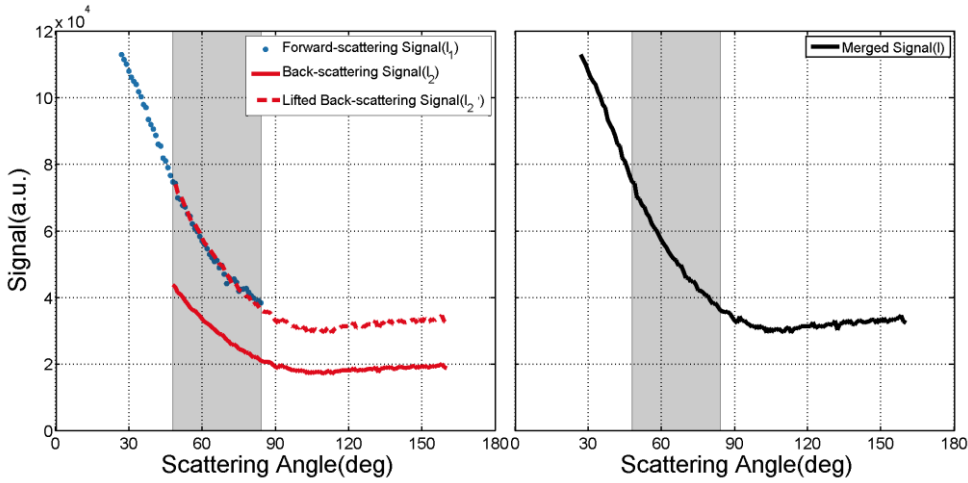


Figure 3: Signal merging of two CCD cameras. Besides the signals captured by the first CCD (blue dotted line) and the second CCD (red solid line), the lifted signal from the second CCD (red dashed line) is also shown in the left drawing. The merged signal is shown in the right drawing.

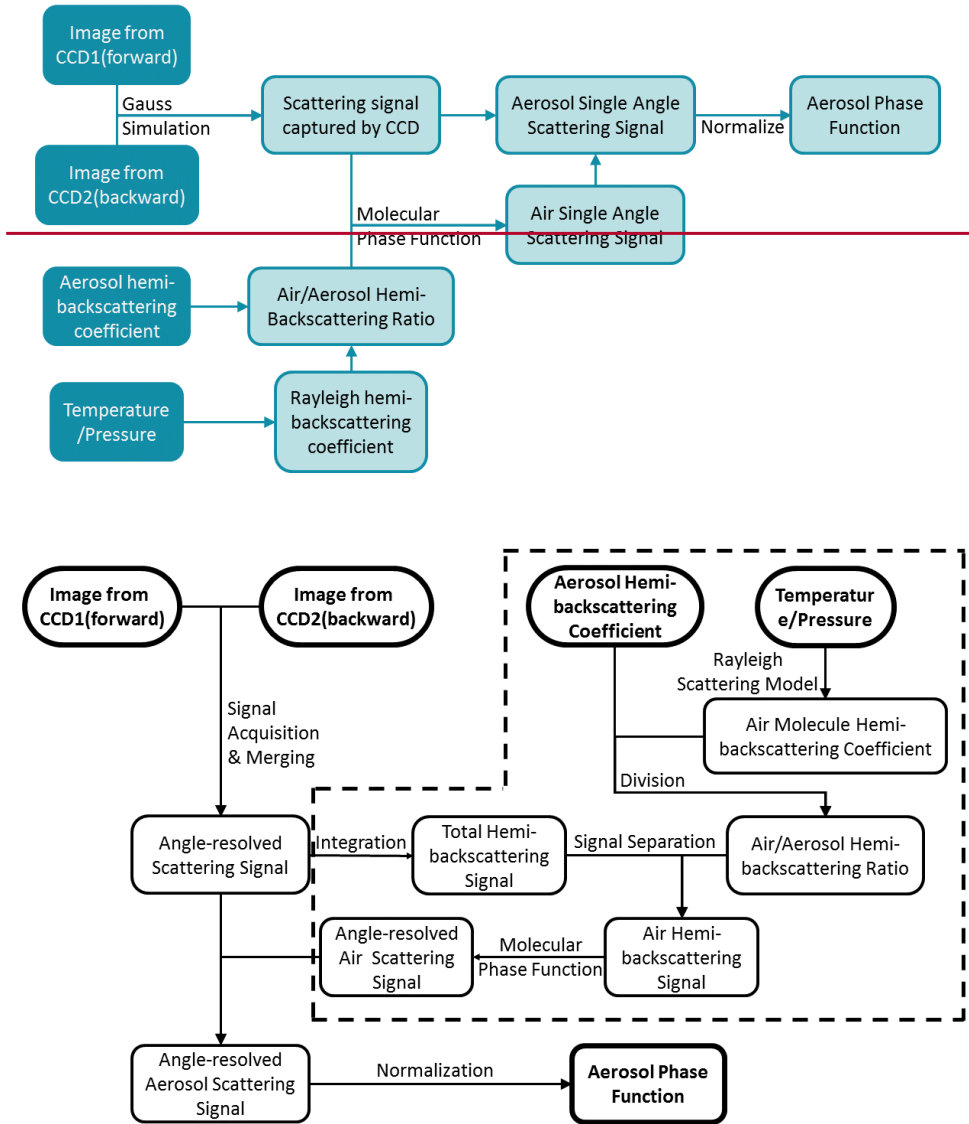


Figure 24: Flow chart of the retrieval algorithm to determine aerosol phase function from CCD-LADS measurements (the processes in the dashed box is used to subtract the scattering signal of air molecules from the total scattering signal)

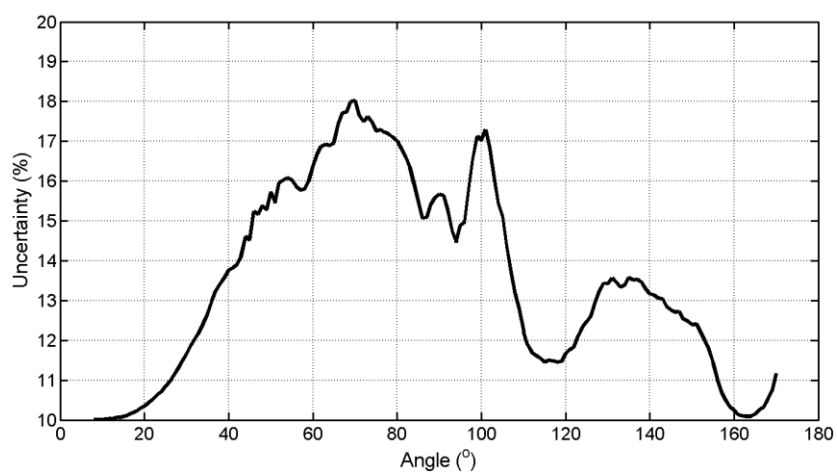


Figure 5: Uncertainties of the merged angle-resolved signal from CCD-LADS measurement

带格式的: 正文, 毕业论文正文, 居中

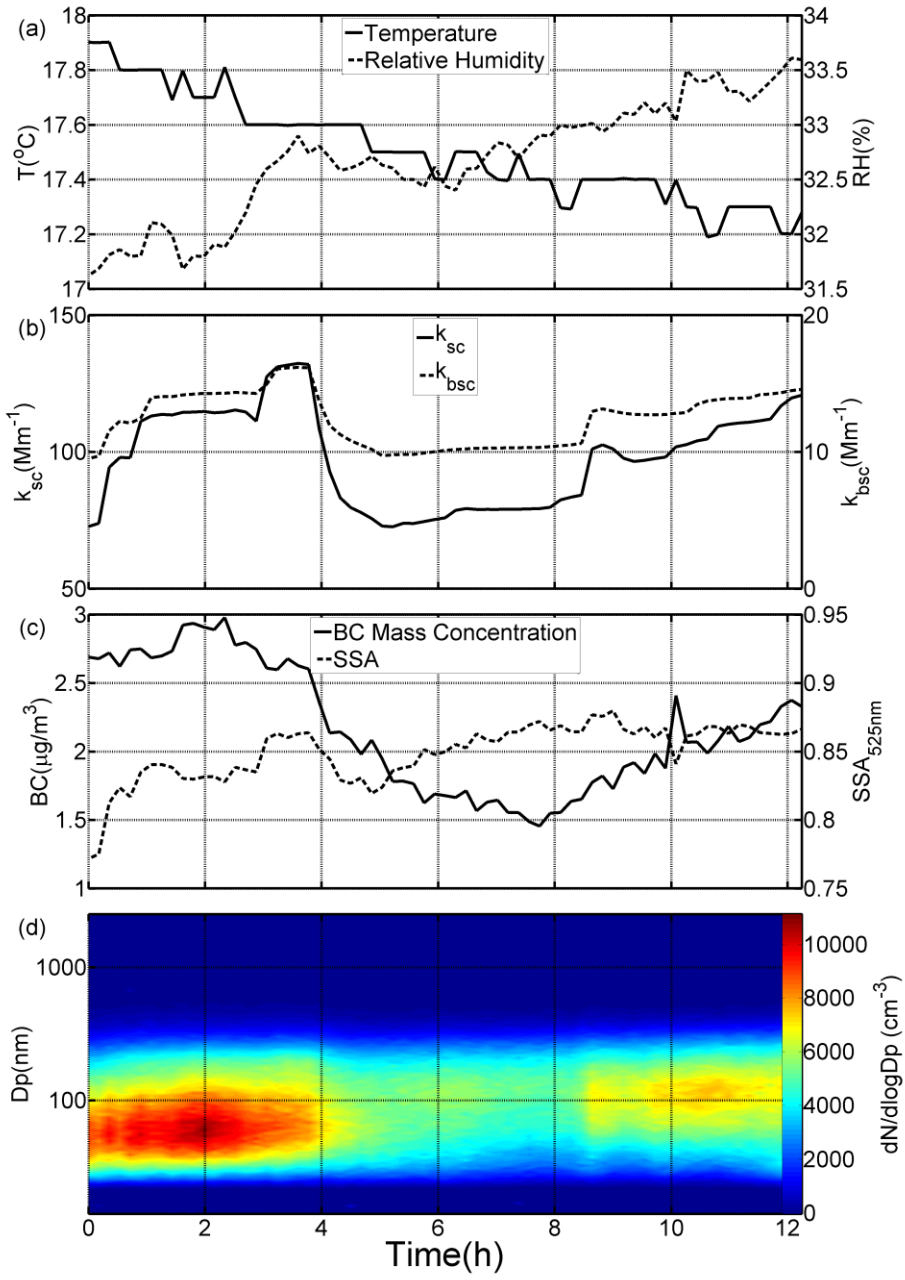


Figure 36: Time series (a) temperature (solid line) and relative humidity (dashed line) in the laboratory, (b) scattering coefficient (solid line) and hemispheric backscattering coefficient (dashed line) of aerosols at 525nm wavelength, (c) mass concentration of black carbon particles (solid line) and single scattering albedo of aerosols at 525nm wavelength (dashed line), (d) PNSD of aerosols during the laboratory study at Peking University in 2015.

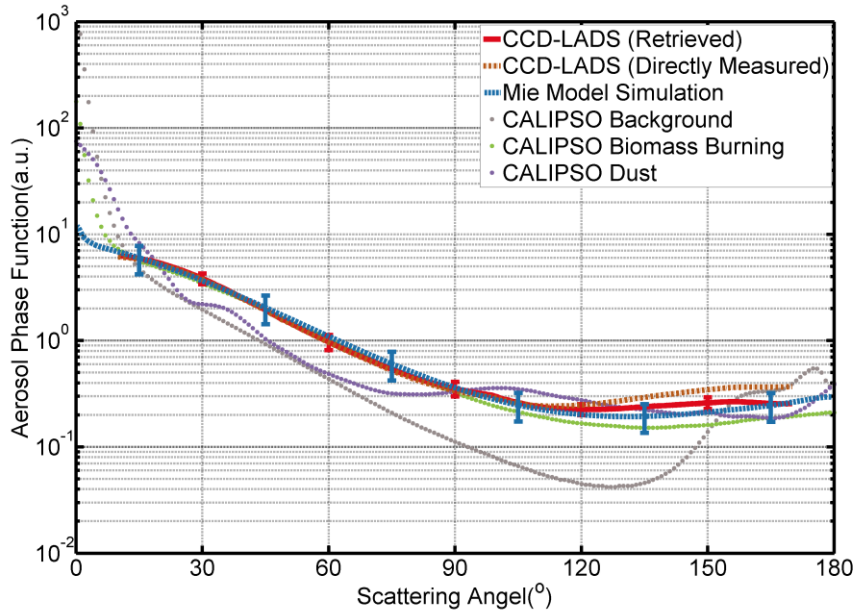


Figure 47: Comparison between aerosol phase function obtained from CCD-LADS measurements (red solid line shows the result estimated with the retrieval algorithm, brown dashed line shows that estimated directly with the measurements), modelled with modified Mie model (blue dashed line) and offered by previous studies with CALIPSO (different colors of dotted lines represent different aerosol types).

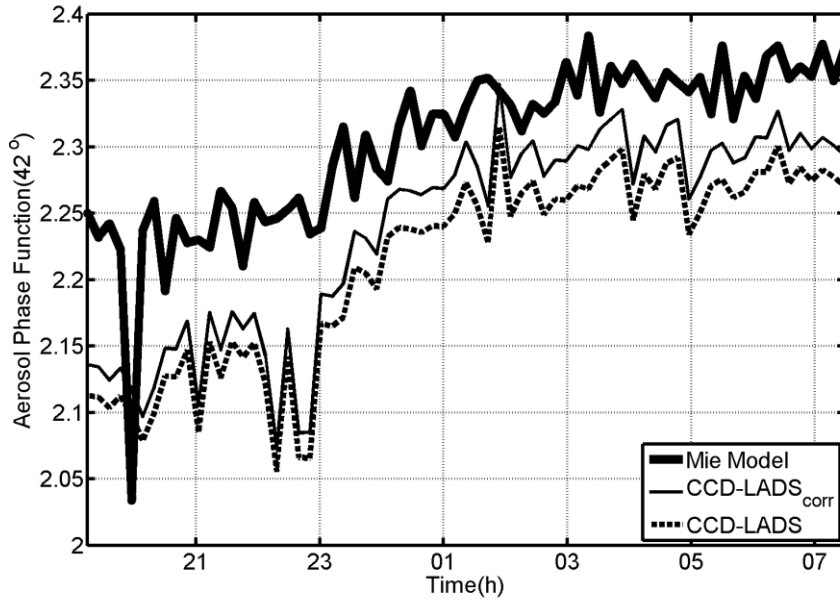


Figure 58: Comparison between aerosol phase function at 42° scattering angle obtained from CCD-LADS measurements (the results estimated with the retrieval algorithm are shown with fine solid line, while the values estimated directly with the measurements are shown with dashed line) and modelled with modified Mie model (shown with bold solid line).

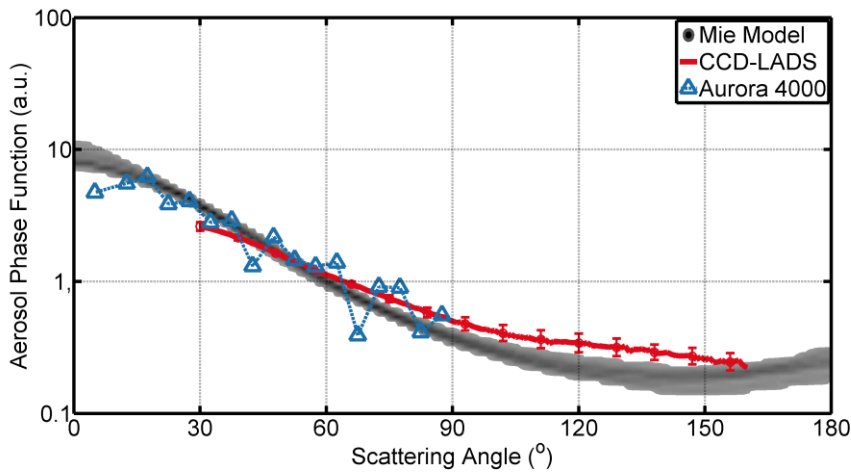


Figure 69: Comparison between aerosol phase function retrieved from CCD-LADS measurements (red line shows the average value, the error bar shows the standard deviation), measured from Aurora 4000 polar nephelometer (blue triangle) and modelled with modified Mie model (grayscale map).